

PROJECTION METHOD FOR QUASIPERIODIC ELLIPTIC EQUATIONS AND APPLICATION TO QUASIPERIODIC HOMOGENIZATION *

KAI JIANG[†], MENG LI[†], JUAN ZHANG[†], AND LEI ZHANG[‡]

Abstract. In this study, our main objective is to address the challenge of solving elliptic equations with quasiperiodic coefficients. To achieve accurate and efficient computation, we introduce the projection method, which enables the embedding of quasiperiodic systems into higher-dimensional periodic systems. To enhance the computational efficiency, we propose a compressed storage strategy for the stiffness matrix by its multi-level block circulant structure, significantly reducing memory requirements. Furthermore, we design a diagonal preconditioner to efficiently solve the resulting high-dimensional linear system by reducing the condition number of the stiffness matrix. These techniques collectively contribute to the computational effectiveness of our proposed approach. Convergence analysis shows the spectral accuracy of our proposed method. We demonstrate the effectiveness and accuracy of our approach through a series of numerical examples. Moreover, we apply our method to achieve a highly accurate computation of the homogenized coefficients for a quasiperiodic multiscale elliptic equation.

Key words. Quasiperiodic elliptic equation, Projection method, Convergence analysis, Multi-level block circulant matrix, Compressed storage, Diagonal preconditioner, Quasiperiodic homogenization.

AMS subject classifications. 65D05, 65D15, 65F08, 35B15, 35B27

1. Introduction. Quasiperiodic systems, such as quasicrystals and Penrose tilings [18, 21, 22], share certain similarities with periodic systems like crystals and periodic tilings, particularly in terms of exhibiting long-range order. Nevertheless, the absence of translational symmetry in quasiperiodic systems, fundamentally distinct from periodic structures, poses challenges in precisely measuring the effective behavior within a representative volume.

Partial differential equations (PDEs) involving quasiperiodic coefficients have been instrumental in describing fascinating phenomena in physics and material science fields, including Moire lattices, magic-angle graphene superlattices, and irrational interfaces [6, 20, 22, 23]. It is of immense significance to deeply research PDEs with quasiperiodic coefficients, as they contribute to revealing essential features and advancing our understanding of complex systems. However, the challenge arises from the fact that quasiperiodic media lacks translation invariance and decay, thereby necessitating the formulation of the corresponding PDE over the entire space. This characteristic presents an essential numerical challenge. Particularly, in homogenization theory, when the microstructures exhibit quasiperiodicity, the asymptotic homogenization techniques [3] for periodic media are extended to quasiperiodic homogenization theory [17, 19, 26]. This extension involves a limit with respect to the entire space, making direct evaluation difficult.

Addressing these challenges and developing effective numerical methods for PDEs with quasiperiodic coefficients is an ongoing area of research, aiming to enable accurate simulations and computations in the presence of quasiperiodic media. The periodic approximation method (PAM) is a conventional approach for approximating quasiperiodic functions, which involves employing a

*Submitted to xxx.

Funding:

[†]Hunan Key Laboratory for Computation and Simulation in Science and Engineering, Key Laboratory of Intelligent Computing and Information Processing of Ministry of Education, School of Mathematics and Computational Science, Xiangtan University, Xiangtan, Hunan, 411105, China (kaijiang@xtu.edu.cn, limeng@smail.xtu.edu.cn, zhangjuan@xtu.edu.cn).

[‡]School of Mathematical Sciences, Institute of Natural Sciences, MOE-LSC, Shanghai Jiao Tong University, Shanghai, 200240, China (lzhang2012@sjtu.edu.cn).

periodic approximation of the quasiperiodic function. In the modified corrector problem, a filter function is incorporated to further enhance the accuracy of PAM [2]. However, the accuracy of PAM is primarily influenced by the Diophantine approximation error [14], which measures the distance between a given real number and its approximate rational number.

In recent years, the projection method (PM) [9, 11] has emerged as a highly accurate and efficient approach for approximating quasiperiodic functions. The PM technique captures the essential characteristics of quasiperiodic functions that can be defined on an irrational manifold of a higher-dimensional torus, allowing for their embedding into higher-dimensional periodic functions. Consequently, PM utilizes the spectral collocation method by employing the discrete Fourier-Bohr transformation to approximate quasiperiodic functions. By efficiently computing higher-dimensional periodic parent functions and incorporating a projection matrix, accurate approximations of quasiperiodic functions can be obtained. Extensive research has confirmed the high accuracy of the PM in computing a diverse range of quasiperiodic systems, including quasicrystals [4, 10], incommensurate quantum systems [8, 12], topological insulators [25], and grain boundaries [7, 13]. Additionally, PM has been proven to possess high accuracy within the quasiperiodic function space and its ability to use the fast Fourier transform (FFT) algorithm to reduce computational complexity [16].

In this study, we introduce a highly efficient algorithm for solving the quasiperiodic elliptic equation within the framework of the PM, accompanied by a thorough convergence analysis. The PM transforms the quasiperiodic elliptic equation from a lower-dimensional problem to a periodic system in a higher dimension, enabling its solution using a pseudo-spectral method. However, this transformation leads to a large linear system with high-dimensional degrees of freedom, posing computational challenges. To tackle the difficulties associated with the large linear system, we introduce a fast algorithm that utilizes a compressed storage format and a diagonal preconditioner. By employing the compressed storage format, we can effectively store and manipulate the tensor product matrices involved in the linear system. This approach enables efficient handling of the memory-intensive matrices arising from the quasiperiodic problem. Furthermore, the diagonal preconditioner is specifically designed to accelerate matrix-vector multiplications, enhancing the overall efficiency of solving the linear system. Through the combination of the compressed storage format and the diagonal preconditioner, our proposed algorithm significantly improves the computational efficiency of solving the quasiperiodic elliptic equation within the PM framework.

To assess the effectiveness of our numerical algorithm and verify our theoretical results, we conduct comprehensive tests on various quasiperiodic elliptic equations. These results demonstrate the remarkable efficiency and spectral accuracy of our method, emphasizing its ability to avoid the Diophantine approximation error [14]. Moreover, we extend the application of our algorithm to compute the homogenized coefficients in a quasiperiodic multiscale problem. By accurately solving the global quasiperiodic corrector equation, our method enables the computation of the homogenized coefficients with spectral accuracy. These outcomes validate the robustness and reliability of our approach in tackling quasiperiodic problems and highlight its potential for a wide range of applications.

Organization. The article is structured as follows. In [Section 2](#), we present an overview of the preliminaries of quasiperiodic function spaces and the quasiperiodic elliptic equation. Moreover, we provide a detailed introduction to the PM. In [Section 3](#), we apply the PM to discretize quasiperiodic elliptic PDEs and provide a rigorous convergence analysis of the proposed method. [Section 4](#) presents a compressed storage method for the stiffness matrix, which significantly reduces storage requirements by utilizing the multilevel block circulant structure, as well as a diagonal preconditioner for the preconditioned conjugate gradient (PCG) method to expedite the computation of the

linear system. In [Section 5](#), we present a series of numerical experiments to validate the accuracy and efficiency of our developed algorithm. These experiments include solving quasiperiodic elliptic equations and computing quasiperiodic homogenized coefficients. Finally, the conclusion and outlook of this paper are given in [Section 6](#).

Notations. We adopt the following notations throughout the paper. For any two numbers a and b , $a \lesssim b$ implies the existence of a constant $C > 0$ such that $a \leq Cb$. Similarly, $a \gtrsim b$ can also be defined. The Hadamard product $(A \circ B)_{ij} = a_{ij}b_{ij}$ represents the element-wise multiplication, denoted as \circ , of two matrices $A = (a_{ij})$, $B = (b_{ij}) \in \mathbb{C}^{n \times n}$. $\|A\|_F := (\sum_{i=1}^n \sum_{j=1}^n |a_{ij}|^2)^{1/2}$ is the Frobenius norm of a matrix $A = (a_{ij}) \in \mathbb{C}^{n \times n}$. For a given number L , $[L]$ denotes the nearest integer to L . The set $\mathcal{D}(n)$ encompasses all diagonal matrices of order n . I_n represents the identity matrix of order n . For a given matrix $\mathbf{P} = (p_{ij}) \in \mathbb{C}^{d \times n}$, its uniform norm $\|\mathbf{P}\|_\infty$ is defined as $\|\mathbf{P}\|_\infty = \max_{1 \leq j \leq n} (\sum_{i=1}^d |p_{ij}|)$. $(\mathbf{e}_i)_{i=1}^n$ is the canonical basis of \mathbb{R}^n .

2. Preliminaries. In this section, we present a brief overview of *quasiperiodic functions* and the concept of *quasiperiodic Sobolev spaces* in [Subsection 2.1](#). This preliminary knowledge is essential for establishing the well-posedness of the *quasiperiodic elliptic equation* introduced in [Subsection 2.2](#). Moreover, we introduce the projection method (PM) in detail in [Subsection 2.3](#).

2.1. Quasiperiodic function space. We start with an n -dimensional periodic function $\mathcal{F}(\mathbf{y})$, $\mathbf{y} \in \mathbb{T}^n = (\mathbb{R}/2\pi\mathbb{Z})^n$. The Fourier series of $\mathcal{F}(\mathbf{y})$ defined on \mathbb{T}^n is

$$(2.1) \quad \mathcal{F}(\mathbf{y}) = \sum_{\mathbf{k} \in \mathbb{Z}^n} \hat{\mathcal{F}}_{\mathbf{k}} e^{i\mathbf{k}^T \mathbf{y}}, \quad \hat{\mathcal{F}}_{\mathbf{k}} = \frac{1}{|\mathbb{T}^n|} \int_{\mathbb{T}^n} \mathcal{F}(\mathbf{y}) e^{-i\mathbf{k}^T \mathbf{y}} d\mathbf{y}, \quad \mathbf{k} \in \mathbb{Z}^n.$$

Next, we introduce the definition and properties of quasiperiodic functions.

DEFINITION 2.1. A matrix $\mathbf{P} \in \mathbb{R}^{d \times n}$ ($d \leq n$) is called the *projection matrix*, if it belongs to the set $\mathbb{P}^{d \times n}$ defined as $\mathbb{P}^{d \times n} := \{\mathbf{P} = (\mathbf{p}_1, \dots, \mathbf{p}_n) \in \mathbb{R}^{d \times n} : \mathbf{p}_1, \dots, \mathbf{p}_n \text{ are } \mathbb{Q}\text{-linearly independent}\}$.

DEFINITION 2.2. A d -dimensional function $f(\mathbf{x})$ is *quasiperiodic*, if there exists an n dimensional periodic function \mathcal{F} and a projection matrix $\mathbf{P} \in \mathbb{P}^{d \times n}$, such that $f(\mathbf{x}) = \mathcal{F}(\mathbf{P}^T \mathbf{x})$ for all $\mathbf{x} \in \mathbb{R}^d$. \mathcal{F} is called the *parent function* of $f(\mathbf{x})$. In particular, when $n = d$ and \mathbf{P} is nonsingular, $f(\mathbf{x})$ is *periodic*. The space of all quasiperiodic functions is denoted as $\text{QP}(\mathbb{R}^d)$.

Let $K_T = \{\mathbf{x} = (x_1, \dots, x_d) \in \mathbb{R}^d : |x_j| \leq T, j = 1, \dots, d\}$. The mean value of $f(\mathbf{x}) \in \text{QP}(\mathbb{R}^d)$ is

$$(2.2) \quad \mathcal{M}\{f(\mathbf{x})\} = \lim_{T \rightarrow \infty} \frac{1}{(2T)^d} \int_{s+K_T} f(\mathbf{x}) d\mathbf{x} := \oint f(\mathbf{x}) d\mathbf{x},$$

where the limit on the right side exists uniformly for all $\mathbf{s} \in \mathbb{R}^d$ [16]. Therefore, calculating the mean value, by definition, involves a limiting process for an integral defined over infinitely increasing domains, which poses a challenge for numerical algorithms.

Through a simple calculation

$$(2.3) \quad \mathcal{M}\left\{e^{i\lambda_1^T \mathbf{x}} e^{-i\lambda_2^T \mathbf{x}}\right\} = \begin{cases} 1, & \lambda_1 = \lambda_2, \\ 0, & \text{otherwise,} \end{cases}$$

and the continuous Fourier transformation

$$(2.4) \quad \hat{f}_{\lambda_{\mathbf{k}}} = \mathcal{M}\left\{f(\mathbf{x}) e^{-i\lambda_{\mathbf{k}}^T \mathbf{x}}\right\},$$

the Fourier series of quasiperiodic function $f(\mathbf{x})$ can be written as

$$(2.5) \quad f(\mathbf{x}) = \sum_{\mathbf{k} \in \mathbb{Z}^n} \hat{f}_{\boldsymbol{\lambda}_{\mathbf{k}}} e^{i\boldsymbol{\lambda}_{\mathbf{k}}^T \mathbf{x}},$$

where $\boldsymbol{\lambda}_{\mathbf{k}} = \mathbf{P}\mathbf{k} \in \Lambda$ are Fourier exponents and $\hat{f}_{\boldsymbol{\lambda}_{\mathbf{k}}}$ are Fourier coefficients. Λ is the spectral point set of $f(\mathbf{x})$.

To clarify the relationship between the Fourier coefficient $\hat{f}_{\boldsymbol{\lambda}_{\mathbf{k}}}$ of the low-dimensional quasiperiodic function and the Fourier coefficient $\hat{\mathcal{F}}_{\mathbf{k}}$ of the higher-dimensional parent function, we present the [Lemma 2.3](#), see also [16, Theorem 4.1], which describes their consistency by invoking the Birkhoff's ergodic theorem [24].

LEMMA 2.3. *For a given quasiperiodic function*

$$f(\mathbf{x}) = \mathcal{F}(\mathbf{P}^T \mathbf{x}), \quad \mathbf{x} \in \mathbb{R}^d,$$

where $\mathcal{F}(\mathbf{y})$ is its parent function defined on \mathbb{T}^n and \mathbf{P} is the projection matrix, we have

$$(2.6) \quad \hat{f}_{\boldsymbol{\lambda}_{\mathbf{k}}} = \hat{\mathcal{F}}_{\mathbf{k}}.$$

Correspondingly, we introduce the notions of periodic function spaces on \mathbb{T}^n and quasiperiodic function spaces on \mathbb{R}^d . Define the Hilbert space: $\mathcal{L}^2(\mathbb{T}^n) = \left\{ \mathcal{F}(\mathbf{y}) : \frac{1}{|\mathbb{T}^n|} \int_{\mathbb{T}^n} |\mathcal{F}|^2 d\mathbf{y} < \infty \right\}$, equipped with inner product

$$(\mathcal{F}_1, \mathcal{F}_2)_{\mathcal{L}^2(\mathbb{T}^n)} = \frac{1}{|\mathbb{T}^n|} \int_{\mathbb{T}^n} \mathcal{F}_1 \bar{\mathcal{F}}_2 d\mathbf{y}.$$

The periodic Sobolev sapce $\mathcal{H}^s(\mathbb{T}^n)$ is defined as

$$\mathcal{H}^s(\mathbb{T}^n) = \left\{ \mathcal{F} \in \mathcal{L}^2(\mathbb{T}^n) : \|\mathcal{F}\|_{\mathcal{H}^s(\mathbb{T}^n)} < \infty \right\}$$

where $\|\mathcal{F}\|_{\mathcal{H}^s(\mathbb{T}^n)} = \left(\sum_{\mathbf{k} \in \mathbb{Z}^n} (1 + |\mathbf{k}|^2)^s |\hat{\mathcal{F}}_{\mathbf{k}}|^2 \right)^{1/2}$, $\hat{\mathcal{F}}_{\mathbf{k}} = (\mathcal{F}, e^{i\mathbf{k}^T \mathbf{y}})_{\mathcal{L}^2(\mathbb{T}^n)}$. The semi-norm of $\mathcal{H}^s(\mathbb{T}^n)$ is given by $|\mathcal{F}|_{\mathcal{H}^s(\mathbb{T}^n)} = \left(\sum_{\mathbf{k} \in \mathbb{Z}^n} |\mathbf{k}|^{2s} |\hat{\mathcal{F}}_{\mathbf{k}}|^2 \right)^{1/2}$.

Define the quasiperiodic Hilbert space:

$$\mathcal{L}_{QP}^2(\mathbb{R}^d) = \left\{ f(\mathbf{x}) \in \text{QP}(\mathbb{R}^d) : \int |f(\mathbf{x})|^2 d\mathbf{x} < \infty \right\}$$

equipped with the inner product and the norm

$$(f_1, f_2)_{\mathcal{L}_{QP}^2(\mathbb{R}^d)} = \int f_1(\mathbf{x}) \bar{f}_2(\mathbf{x}) d\mathbf{x}, \quad \|f\|_{\mathcal{L}_{QP}^2(\mathbb{R}^d)} = (f, f)_{\mathcal{L}_{QP}^2(\mathbb{R}^d)}^{1/2},$$

and

$$\mathcal{L}_{QP}^\infty(\mathbb{R}^d) = \left\{ f(\mathbf{x}) \in \text{QP}(\mathbb{R}^d) : \|f\|_{\mathcal{L}_{QP}^\infty(\mathbb{R}^d)} = \sup_{\mathbf{x} \in \mathbb{R}^d} |f(\mathbf{x})| < \infty \right\}.$$

We have the Parseval's identity with respect to the $\mathcal{L}_{QP}^2(\mathbb{R}^d)$ -norm,

$$(2.7) \quad \|f\|_{\mathcal{L}_{QP}^2(\mathbb{R}^d)}^2 = \mathcal{M} \{ |f(\mathbf{x})|^2 \} = \sum_{\mathbf{k} \in \mathbb{Z}^n} |\hat{f}_{\lambda_{\mathbf{k}}}|^2.$$

Furthermore, for any $s \in \mathbb{N}^+$, the s -derivative quasiperiodic Sobolev space $\mathcal{H}_{QP}^s(\mathbb{R}^d)$ is defined through the following inner product

$$(f_1, f_2)_{\mathcal{H}_{QP}^s(\mathbb{R}^d)} = (f_1, f_2)_{\mathcal{L}_{QP}^2(\mathbb{R}^d)} + \sum_{|p| \leq s} (\partial_{\mathbf{x}}^p f_1, \partial_{\mathbf{x}}^p f_2)_{\mathcal{L}_{QP}^2(\mathbb{R}^d)},$$

and the corresponding norm

$$\|f\|_{\mathcal{H}_{QP}^s(\mathbb{R}^d)}^2 = \sum_{\lambda \in \Lambda} (1 + |\lambda|^2)^s |\hat{f}_{\lambda}|^2.$$

The $\mathcal{H}_{QP}^s(\mathbb{R}^d)$ semi-norm is defined as

$$|f|_{\mathcal{H}_{QP}^s(\mathbb{R}^d)}^2 = \sum_{|p|=s} (\partial_{\mathbf{x}}^p f, \partial_{\mathbf{x}}^p f)_{\mathcal{L}_{QP}^2(\mathbb{R}^d)} = \sum_{\lambda \in \Lambda} |\lambda|^{2s} |\hat{f}_{\lambda}|^2.$$

For the case of $s = 0$, we have $\mathcal{H}_{QP}^0(\mathbb{R}^d) = \mathcal{L}_{QP}^2(\mathbb{R}^d)$. To simplify notation, we use $\|\cdot\|_0$ to denote the norm $\|\cdot\|_{\mathcal{L}_{QP}^2(\mathbb{R}^d)}$, $\|\cdot\|_s$ to denote the norm $\|\cdot\|_{\mathcal{H}_{QP}^s(\mathbb{R}^d)}$.

2.2. Quasiperiodic elliptic equations. With the preparation in the previous subsection, we introduce the quasiperiodic elliptic equation and discuss its well-posedness. Consider the following equation

$$(2.8) \quad \mathcal{L}u(\mathbf{x}) = f(\mathbf{x}), \quad \mathbf{x} \in \mathbb{R}^d,$$

where the second order elliptic operator $\mathcal{L} : \mathcal{H}_{QP}^1(\mathbb{R}^d) \rightarrow \mathcal{L}_{QP}^2(\mathbb{R}^d)$ is defined as

$$\mathcal{L}u(\mathbf{x}) = -\operatorname{div}(\alpha(\mathbf{x})\nabla u(\mathbf{x})).$$

Here, the coefficient $\alpha(\mathbf{x}) \in \mathcal{L}_{QP}^\infty(\mathbb{R}^d)$ and the source term $f(\mathbf{x}) \in \mathcal{L}_{QP}^2(\mathbb{R}^d)$. Furthermore, $\alpha(\mathbf{x})$ is uniformly elliptic and bounded, that is, for all $\mathbf{x}, \xi \in \mathbb{R}^d$,

$$\gamma_0 |\xi|^2 \leq \xi^T \alpha(\mathbf{x}) \xi \leq \gamma_1 |\xi|^2, \quad \gamma_0, \gamma_1 > 0.$$

By multiplying (2.8) with an arbitrary test function $v \in \mathcal{H}_{QP}^1(\mathbb{R}^d)$ and integrating over \mathbb{R}^d , we can apply an integration by parts, taking into account that the boundary integral vanishes (see [15, Lemma 3.4]). This leads to the following expression

$$(\alpha \nabla u, \nabla v) = (f, v),$$

where the bilinear form $\alpha(\cdot, \cdot) : \mathcal{H}_{QP}^1(\mathbb{R}^d) \times \mathcal{H}_{QP}^1(\mathbb{R}^d) \rightarrow \mathbb{R}$ is defined as

$$\alpha(u, v) := (\alpha \nabla u, \nabla v), \quad u, v \in \mathcal{H}_{QP}^1(\mathbb{R}^d).$$

The associated variational formulation of (2.8) is to seek $u \in \mathcal{H}_{QP}^1(\mathbb{R}^d)$ such that

$$(2.9) \quad \alpha(u, v) = (f, v), \quad \forall v \in \mathcal{H}_{QP}^1(\mathbb{R}^d).$$

The solution to (2.9) is not unique and can be determined up to a constant. To address the non-uniqueness of the solution, we impose the assumption that u has a mean value of zero. This allows us to define the space

$$\overline{\mathcal{H}}_{QP}^1(\mathbb{R}^d) := \left\{ u(\mathbf{x}) \in \mathcal{H}_{QP}^1(\mathbb{R}^d) : \oint u(\mathbf{x}) d\mathbf{x} = 0 \right\}$$

equipped with $\mathcal{H}_{QP}^1(\mathbb{R}^d)$ -norm. We apply the Lax-Milgram Lemma in $\overline{\mathcal{H}}_{QP}^1(\mathbb{R}^d)$ to establish the uniqueness of the weak solution.

THEOREM 2.4. *There exists a unique solution of problem*

$$(2.10) \quad u \in \overline{\mathcal{H}}_{QP}^1(\mathbb{R}^d), \quad \alpha(u, v) = (f, v), \quad \forall v \in \overline{\mathcal{H}}_{QP}^1(\mathbb{R}^d).$$

Before proving Theorem 2.4, we introduce two lemmas that are required for the proof. The first lemma is the equivalent modulus theorem [1] (Lemma A.1), and the second lemma is Poincaré's inequality (Lemma B.1). Detailed proofs of these two lemmas are provided in Appendix A and Appendix B, respectively. Then we give the proof of Theorem 2.4.

Proof. According to the Lax-Milgram theorem, to establish the existence and uniqueness of the solution for problem (2.10), we need to justify the boundedness and coercivity of the bilinear form $\alpha(\cdot, \cdot)$. The boundedness follows from

$$(2.11) \quad |\alpha(u, v)| \leq \gamma_1 \left| \oint_{\mathbb{R}^d} \nabla u \overline{\nabla v} d\mathbf{x} \right| \lesssim |u|_1 |v|_1 \lesssim \|u\|_1 \|v\|_1.$$

Using Lemma B.1, we have

$$(2.12) \quad |\alpha(u, u)| \geq \gamma_0 \left| \oint_{\mathbb{R}^d} \nabla u \overline{\nabla u} d\mathbf{x} \right| \gtrsim |u|_1 |u|_1 \gtrsim \|u\|_1^2,$$

which implies that $\alpha(\cdot, \cdot)$ is coercive. \square

2.3. Projection method. In this subsection, we provide a detailed introduction to the PM. PM is an accurate and efficient approach for solving quasiperiodic systems. This method involves transforming the quasiperiodic function $f(\mathbf{x})$ into a high-dimensional periodic function $\mathcal{F}(\mathbf{y})$. By doing so, we can directly substitute the discrete quasiperiodic Fourier coefficients with the discrete Fourier coefficients of parent function. Consequently, the PM benefits from the efficiency of the FFT algorithm.

For an integer $N \in \mathbb{N}^+$ and a given projection matrix $\mathbf{P} \in \mathbb{P}^{d \times n}$, denote

$$K_N^n = \left\{ \mathbf{k} = (k_j)_{j=1}^n \in \mathbb{Z}^n : -N/2 \leq k_j < N/2 \right\}.$$

Next, we discretize the torus \mathbb{T}^n as

$$\mathbb{T}_N^n = \left\{ \mathbf{y}_j = (2\pi j_1/N, \dots, 2\pi j_n/N) \in \mathbb{T}^n : 0 \leq j_1, \dots, j_n < N, \mathbf{j} = (j_1, \dots, j_n) \right\}.$$

Namely, we distribute N discrete points uniformly in each spatial direction of the n -dimensional space. Consequently, there are $D = N^n$ discrete points in total. We denote the grid function space as

$$S_N = \{\mathcal{F} : \mathbb{Z}^n \mapsto \mathbb{C}, \mathcal{F} \text{ is periodic on } \mathbb{T}_N^n\}$$

and define the ℓ^2 -inner product $(\cdot, \cdot)_N$ on S_N as

$$(\phi_1, \phi_2)_N = \frac{1}{D} \sum_{\mathbf{y}_j \in \mathbb{T}_N^n} \phi_1(\mathbf{y}_j) \bar{\phi}_2(\mathbf{y}_j), \quad \phi_1, \phi_2 \in S_N.$$

For $\mathbf{k}_1, \mathbf{k}_2 \in \mathbb{Z}^n$, $\mathbf{P} \in \mathbb{P}^{d \times n}$, we denote $\mathbf{P}\mathbf{k}_1 \stackrel{N}{=} \mathbf{P}\mathbf{k}_2$, if $\mathbf{P}\mathbf{k}_1 = \mathbf{P}\mathbf{k}_2 + N\mathbf{P}\mathbf{m}$, $N \in \mathbb{Z}$, $\mathbf{m} \in \mathbb{Z}^n$. In particular, if $\mathbf{P} = I_n$, $\mathbf{k}_1 \stackrel{N}{=} \mathbf{k}_2$ implies $\mathbf{k}_1 = \mathbf{k}_2 + N\mathbf{m}$. We have the following discrete orthogonality

$$(2.13) \quad \left(e^{i\mathbf{k}_1^T \mathbf{y}_j}, e^{i\mathbf{k}_2^T \mathbf{y}_j} \right)_N = \begin{cases} 1, & \mathbf{k}_1 \stackrel{N}{=} \mathbf{k}_2, \\ 0, & \text{otherwise.} \end{cases}$$

Consequently, we can compute the discrete Fourier coefficients of a high-dimensional periodic function $F(\mathbf{y})$ as follows

$$\tilde{\mathcal{F}}_{\mathbf{k}} = \left(\mathcal{F}(\mathbf{y}_j), e^{i\mathbf{k}^T \mathbf{y}_j} \right)_N = \frac{1}{D} \sum_{\mathbf{y}_j \in \mathbb{T}_N^n} \mathcal{F}(\mathbf{y}_j) e^{-i\mathbf{k}^T \mathbf{y}_j}.$$

From the [Lemma 2.3](#), PM directly takes

$$(2.14) \quad \tilde{f}_{\lambda_{\mathbf{k}}} = \tilde{\mathcal{F}}_{\mathbf{k}},$$

which allows us to numerically simulate low-dimensional quasiperiodic functions using information from high-dimensional parent functions. Therefore, we can define the *discrete Fourier-Bohr transform* of a quasiperiodic function $f(\mathbf{x})$ as follows

$$(2.15) \quad f(\mathbf{x}_j) = \sum_{\lambda_{\mathbf{k}} \in \Lambda_N^d} \tilde{f}_{\lambda_{\mathbf{k}}} e^{i\lambda_{\mathbf{k}}^T \mathbf{x}_j}, \quad \Lambda_N^d = \{\lambda_{\mathbf{k}} : \lambda_{\mathbf{k}} = \mathbf{P}\mathbf{k}, \mathbf{k} \in K_N^n\},$$

where $\mathbf{x}_j \in X_{\mathbf{P}} := \{\mathbf{x}_j = \mathbf{P}\mathbf{y}_j : \mathbf{y}_j \in \mathbb{T}_N^n, \mathbf{P} \in \mathbb{P}^{d \times n}\}$ are *collocation points*. The truncation of a quasiperiodic function f is defined as

$$T_N f(\mathbf{x}) = \sum_{\lambda_{\mathbf{k}} \in \Lambda_N^d} \hat{f}_{\lambda_{\mathbf{k}}} e^{i\lambda_{\mathbf{k}}^T \mathbf{x}} := u_T(\mathbf{x}),$$

and the trigonometric interpolation of f is given by

$$I_N f(\mathbf{x}) = \sum_{\lambda_{\mathbf{k}} \in \Lambda_N^d} \tilde{f}_{\lambda_{\mathbf{k}}} e^{i\lambda_{\mathbf{k}}^T \mathbf{x}} := u_I(\mathbf{x}).$$

Consequently, $f(\mathbf{x}_j) = I_N f(\mathbf{x}_j)$. From a computational perspective, it is apparent that the PM can use the multidimensional FFT algorithm to obtain the Fourier coefficients of a quasiperiodic function.

3. Application of PM to quasiperiodic elliptic PDEs and convergence analysis. In this section, we present the PM for the numerical solution of quasiperiodic elliptic equations. We derive the corresponding discrete scheme and linear system for (2.8) by using the tensor-vector-index conversion technique. Moreover, we provide a rigorous convergence analysis for the PM method in solving quasiperiodic elliptic PDEs.

3.1. PM discretization of quasiperiodic elliptic PDEs. In this subsection, we discretize equation (2.8) using the PM. We then develop a discrete scheme based on the variational formulation and generate the corresponding linear system using index conversion.

3.1.1. Discrete scheme. Within the PM framework, we can discretize $\alpha(\mathbf{x})$ and $f(\mathbf{x})$ in (2.8) as follows

$$\begin{aligned}\alpha(\mathbf{x}_j) &= \sum_{\boldsymbol{\lambda}_\alpha \in \Lambda_{\alpha,N}^d} \tilde{\alpha}_{\boldsymbol{\lambda}_\alpha} e^{i\boldsymbol{\lambda}_\alpha^T \mathbf{x}_j}, \quad \tilde{\alpha}_{\boldsymbol{\lambda}_\alpha} = \tilde{\mathcal{A}}_{\mathbf{k}_\mathcal{A}} = \frac{1}{D} \sum_{\mathbf{y}_j \in \mathbb{T}_N^n} \mathcal{A}(\mathbf{y}_j) e^{-i\mathbf{k}_\mathcal{A}^T \mathbf{y}_j}, \quad \mathbf{x}_j \in X_P, \\ f(\mathbf{x}_j) &= \sum_{\boldsymbol{\lambda}_f \in \Lambda_{f,N}^d} \tilde{f}_{\boldsymbol{\lambda}_f} e^{i\boldsymbol{\lambda}_f^T \mathbf{x}_j}, \quad \tilde{f}_{\boldsymbol{\lambda}_f} = \tilde{\mathcal{F}}_{\mathbf{k}_\mathcal{F}} = \frac{1}{D} \sum_{\mathbf{y}_j \in \mathbb{T}_N^n} \mathcal{F}(\mathbf{y}_j) e^{-i\mathbf{k}_\mathcal{F}^T \mathbf{y}_j}, \quad \mathbf{x}_j \in X_P,\end{aligned}$$

where \mathcal{A}, \mathcal{F} are parent functions of α, f , respectively. A simple calculation reveals that the spectral points of u satisfy $\boldsymbol{\lambda}_u = \boldsymbol{\lambda}_f - \boldsymbol{\lambda}_\alpha$, which means that the spectral point set of u is spanned by the spectral point sets of α and f . Based on this, we can determine the set

$$\Lambda_{u,N}^d \subseteq \text{span}_{\mathbb{Z}} \{ \Lambda_{\alpha,N}^d, \Lambda_{f,N}^d \} := \{ k_1 \boldsymbol{\lambda}_\alpha + k_2 \boldsymbol{\lambda}_f : \boldsymbol{\lambda}_\alpha \in \Lambda_{\alpha,N}^d, \boldsymbol{\lambda}_f \in \Lambda_{f,N}^d, k_1, k_2 \in \mathbb{Z} \}$$

and discretize $u(\mathbf{x})$ as

$$u(\mathbf{x}_j) = \sum_{\boldsymbol{\lambda}_u \in \Lambda_{u,N}^d} \tilde{u}_{\boldsymbol{\lambda}_u} e^{i\boldsymbol{\lambda}_u^T \mathbf{x}_j}, \quad \tilde{u}_{\boldsymbol{\lambda}_u} = \tilde{\mathcal{U}}_{\mathbf{k}_u} = \frac{1}{D} \sum_{\mathbf{y}_j \in \mathbb{T}_N^n} \mathcal{U}(\mathbf{y}_j) e^{-i\mathbf{k}_u^T \mathbf{y}_j}, \quad \mathbf{x}_j \in X_P,$$

where \mathcal{U} is the parent function of u .

REMARK 3.1. We provide a simple example to illustrate how the spectral point set $\Lambda_{u,N}^d$ is spanned. Let $\Lambda_{\alpha,N}^d \subseteq \mathbb{Z}(1, \sqrt{2})$ and $\Lambda_{f,N}^d \subseteq \mathbb{Z}(1, \sqrt{3})$, where $\mathbb{Z}(1, \sqrt{2})$ represents the spectral point set formed by integer linear combinations of 1 and $\sqrt{2}$, and similarly for $\mathbb{Z}(1, \sqrt{3})$. In this case, $\Lambda_{u,N}^d$ can be spanned by these two spectral point sets, which can be expressed as follows

$$\Lambda_{u,N}^d \subseteq \text{span}_{\mathbb{Z}} \{ \Lambda_{\alpha,N}^d, \Lambda_{f,N}^d \} = \mathbb{Z}(1, \sqrt{2}, \sqrt{3}).$$

Let $V^N := \text{span}\{e^{i\boldsymbol{\lambda}_v^T \mathbf{x}} : \boldsymbol{\lambda}_v \in \Lambda_{u,N}^d, \mathbf{x} \in \mathbb{R}^d\}$ be a finite-dimensional subspace of $\text{QP}(\mathbb{R}^d)$. We then select a test function v from the space $\bar{V}^N := \{v \in V^N : \tilde{v}_0 = 0\} \subseteq \bar{\mathcal{H}}_{QP}^1(\mathbb{R}^d)$. In the following, our goal is to find an approximate solution of (2.10) in \bar{V}^N , i.e., $u \in \bar{V}^N$, such that

$$(3.1) \quad \alpha_N(u, v) := (\alpha \nabla u, \nabla v)_N = (f, v)_N, \quad \forall v \in \bar{V}^N.$$

REMARK 3.2. The discrete variational formulation (3.1), which is associated with the discrete problem (3.9) introduced in Subsection 3.2, is shown in Appendix C to have a unique solution.

In view of the discrete orthogonality of quasiperiodic base functions

$$(3.2) \quad \left(e^{i\lambda_1^T \mathbf{x}_j}, e^{i\lambda_2^T \mathbf{x}_j} \right)_N = \begin{cases} 1, & \lambda_1 \stackrel{N}{=} \lambda_2, \\ 0, & \text{otherwise,} \end{cases}$$

we have

$$\begin{aligned} (\alpha \nabla u, \nabla v)_N &= \sum_{\lambda_u \in \Lambda_{u,N}^d} \tilde{\alpha}_{\lambda_v - \lambda_u} (\lambda_v^T \lambda_u) \tilde{u}_{\lambda_u}, \\ (f, v)_N &= \tilde{f}_{\lambda_v}. \end{aligned}$$

Combining with (2.14), we can derive the discrete scheme for (2.8) as follows

$$(3.3) \quad \sum_{\mathbf{k}_{\mathcal{U}} \in K_N^n} \tilde{\mathcal{A}}_{\mathbf{k}_{\mathcal{A}}} (\mathbf{P} \mathbf{k}_{\mathcal{V}})^T (\mathbf{P} \mathbf{k}_{\mathcal{U}}) \tilde{\mathcal{U}}_{\mathbf{k}_{\mathcal{U}}} = \tilde{\mathcal{F}}_{\mathbf{k}_{\mathcal{V}}}, \quad \mathbf{k}_{\mathcal{A}} = \mathbf{k}_{\mathcal{V}} - \mathbf{k}_{\mathcal{U}},$$

where $\mathbf{k}_{\mathcal{V}} - \mathbf{k}_{\mathcal{U}} := (\mathbf{k}_{\mathcal{V}} - \mathbf{k}_{\mathcal{U}}) \pmod{N}$. Note that for a given vector $\mathbf{k} = (k_1, \dots, k_n) \in \mathbb{Z}^n$, we have $\mathbf{k} \pmod{N} \equiv (k_1 \pmod{N}, \dots, k_n \pmod{N})$.

3.1.2. Linear system. The discrete scheme (3.3) is formulated with respect to the tensor index $\mathbf{k} = (k_1, \dots, k_n) \in K_N^n$. To solve it numerically, we introduce a general index conversion between tensors and vectors to obtain a matrix linear system.

For a given tensor $\mathcal{I} \in \mathbb{C}^{N_1 \times \dots \times N_n}$, we denote its size vector as

$$\mathbf{N} = (N_k)_{k=1}^n, \quad N_k \in \mathbb{N}^+$$

and the set

$$K_N^n = \{\mathbf{i} = (i_k)_{k=1}^n \in \mathbb{Z}^n : -N_k/2 \leq i_k < N_k/2\}.$$

Let $\mathbf{i} = (i_1, \dots, i_n) \in K_N^n$ be the index of \mathcal{I} . Define the *convert bijection* as follows

$$(3.4) \quad \begin{aligned} \mathcal{C} : K_N^n &\rightarrow \mathbb{N}, \\ \mathbf{i} &\xrightarrow{\mathcal{C}} i, \end{aligned}$$

where i is determined by the rule

$$(3.5) \quad i = \sum_{k=1}^n \bar{i}_k \prod_{t=k+1}^n N_t, \quad \bar{i}_k := i_k \pmod{N_k}.$$

The index inverse conversion \mathcal{C}^{-1} is defined by

$$(3.6) \quad i_k = \begin{cases} \bar{i}_k, & 0 \leq \bar{i}_k < N_k/2, \\ \bar{i}_k - N_k, & N_k/2 \leq \bar{i}_k < N_k, \end{cases} \quad \bar{i}_k = \left\lfloor i \pmod{\prod_{t=k}^n N_t} / \prod_{t=k+1}^n N_t \right\rfloor,$$

where $\lfloor \cdot \rfloor$ is the floor symbol. We refer to the bijection \mathcal{C} as the tensor-vector-index conversion.

Next, we generate the linear system using (3.4), assuming $N_k = N$ for each k . Define

$$A = (A_{ij}) \in \mathbb{C}^{D \times D}, \quad A_{ij} = \tilde{\mathcal{A}}_{\mathbf{k}_{\mathcal{V}} - \mathbf{k}_{\mathcal{U}}},$$

$$W = (W_{ij}) \in \mathbb{C}^{D \times D}, \quad W_{ij} = (\mathbf{P}\mathbf{k}_V)^T (\mathbf{P}\mathbf{k}_U),$$

where indices i, j are determined by

$$(3.7) \quad \mathbf{k}_V \xrightarrow{\mathcal{C}} i, \quad \mathbf{k}_U \xrightarrow{\mathcal{C}} j,$$

respectively. And the column vectors \mathbf{U} and \mathbf{F} are defined, respectively, by

$$\mathbf{U} = (U_j) \in \mathbb{C}^D, \quad U_j = \tilde{\mathcal{U}}_{\mathbf{k}_U},$$

$$\mathbf{F} = (F_i) \in \mathbb{C}^D, \quad F_i = \tilde{\mathcal{F}}_{\mathbf{k}_V}.$$

Consequently, we obtain the following linear system

$$(3.8) \quad Q\mathbf{U} = \mathbf{F}, \quad Q = A \circ W \in \mathbb{C}^{D \times D}.$$

REMARK 3.3. As N and n increase, the size of the matrix $Q \in \mathbb{C}^{D \times D}$, grows excessively large, leading to a substantial increase in computational cost and memory requirements. Meanwhile, as the size of Q increases, the linear system becomes ill-conditioned, slowing convergence with standard iterative methods. To address these challenges, in [Section 4](#), we will propose a compressed storage method for reducing memory usage and an efficient preconditioner in solving the linear system (3.8).

3.2. Convergence analysis. In this subsection, we provide a thorough convergence analysis of PM for solving the quasiperiodic elliptic equation (2.8).

3.2.1. Main theorem. Let u be the solution of problem (2.8), and u_N the solution of the corresponding discrete problem

$$(3.9) \quad \tilde{\mathcal{L}}u = f_I,$$

where the operator $\tilde{\mathcal{L}}$ is defined by

$$(3.10) \quad \tilde{\mathcal{L}}u := -\operatorname{div}(I_N(\alpha \nabla u)).$$

We now present the main result of error analysis.

THEOREM 3.1. Let $s \geq 1$. There exists a constant C such that for $f \in \mathcal{L}_{QP}^2(\mathbb{R}^d)$ and $u \in \bar{\mathcal{H}}_{QP}^1(\mathbb{R}^d)$, with their parent functions $\mathcal{F} \in \mathcal{H}^s(\mathbb{T}^n)$, $\mathcal{U} \in \mathcal{H}^{s+1}(\mathbb{T}^n)$, if the following regularity condition is satisfied

$$(3.11) \quad \|\mathcal{U}\|_{\mathcal{H}^{s+1}(\mathbb{T}^n)} \leq C \|\mathcal{F}\|_{\mathcal{H}^s(\mathbb{T}^n)},$$

then the error estimate is

$$\|u - u_N\|_0 \leq CN^{-s} \|\mathcal{F}\|_{\mathcal{H}^s(\mathbb{T}^n)}.$$

Sketch of proof. Using the triangle inequality, we can decompose the numerical error $\|u - u_N\|_0$ into two components: the truncation error $\|u - u_T\|_0$ and the aliasing error $\|u_T - u_N\|_0$. Here u_T refers to the truncation of the solution u to the (2.8). The truncation error can be derived from [Lemma 3.2](#) in [Subsection 3.2.2](#). Subsequently, we establish an upper bound for the aliasing error in [Lemma 3.4](#). Finally, the proof of the main result is completed in [Subsection 3.2.3](#).

3.2.2. Some results. Before proving the main conclusion, we present some essential results.

Lemma 3.2 provides the truncation error estimate of quasiperiodic functions and a rigorous convergence result for the PM, as also presented in [16, Theorem 5.1] and [16, Theorem 5.3], respectively.

LEMMA 3.2. *Suppose that $f(\mathbf{x}) \in \text{QP}(\mathbb{R}^d)$ and its parent function $\mathcal{F}(\mathbf{y}) \in \mathcal{H}^s(\mathbb{T}^n)$ with $s \geq 0$. There exists a constant C , independent of \mathcal{F} and N , such that*

$$(3.12) \quad \|T_N f - f\|_0 \leq CN^{-s} |\mathcal{F}|_{\mathcal{H}^s(\mathbb{T}^n)},$$

$$(3.13) \quad \|I_N f - f\|_0 \leq CN^{-s} |\mathcal{F}|_{\mathcal{H}^s(\mathbb{T}^n)}.$$

Using this lemma, we estimate the truncation and interpolation errors of the gradient of quasiperiodic functions in **Lemma 3.3**.

LEMMA 3.3. *For $s \geq 1$, there exists a constant C such that if $u \in \mathcal{H}_{QP}^1(\mathbb{R}^d)$ and its parent function $\mathcal{U} \in \mathcal{H}^{s+1}(\mathbb{T}^n)$, then the inequality holds:*

$$(3.14) \quad \|T_N(\alpha \nabla u) - \alpha \nabla u\|_0 \leq CN^{-s} \|\mathcal{U}\|_{\mathcal{H}^{s+1}(\mathbb{T}^n)},$$

$$(3.15) \quad \|I_N(\alpha \nabla u) - \alpha \nabla u\|_0 \leq CN^{-s} \|\mathcal{U}\|_{\mathcal{H}^{s+1}(\mathbb{T}^n)}.$$

Proof. Let $\phi(\mathbf{x}) = \alpha(\mathbf{x}) \nabla u(\mathbf{x}) \in \text{QP}(\mathbb{R}^d)$. The parent function of ϕ , denoted as Φ , is expressed as

$$\Phi(\mathbf{y}) = \mathcal{A}(\mathbf{y}) \tilde{\nabla} \mathcal{U}(\mathbf{y}),$$

where $\tilde{\nabla}$ is given by $\tilde{\nabla} = \left(\sum_{i=1}^d p_{i1} \frac{\partial}{\partial y_1}, \dots, \sum_{i=1}^d p_{in} \frac{\partial}{\partial y_n} \right)$. Combining this with the **Lemma 3.2**, we have

$$\begin{aligned} \|T_N \phi - \phi\|_0 &\leq C_2 N^{-s} \|\Phi\|_{\mathcal{H}^s(\mathbb{T}^n)} \\ &\leq C_2 N^{-s} \left(\sup_{\mathbf{y} \in \mathbb{T}^n} |\mathcal{A}| \right) \|\tilde{\nabla} \mathcal{U}\|_{\mathcal{H}^s(\mathbb{T}^n)} \\ &\leq C_1 N^{-s} \|\mathbf{P}\|_{\infty} \|\nabla \mathcal{U}\|_{\mathcal{H}^s(\mathbb{T}^n)} \\ &\leq CN^{-s} \|\mathcal{U}\|_{\mathcal{H}^{s+1}(\mathbb{T}^n)}, \end{aligned}$$

where C, C_1, C_2 are positive constants, and $\nabla \mathcal{U} = \left(\frac{\partial \mathcal{U}}{\partial y_1}, \dots, \frac{\partial \mathcal{U}}{\partial y_n} \right)$. This implies that inequality (3.14) holds.

Similarly, by using (3.13), we have the following estimate

$$\|I_N \phi - \phi\|_0 \leq CN^{-s} \|\mathcal{U}\|_{\mathcal{H}^{s+1}(\mathbb{T}^n)},$$

which implies the (3.15) holds. \square

Using **Lemma 3.2** and **Lemma 3.3**, we can estimate the upper bound for the aliasing error $\|u_T - u_N\|_0$.

LEMMA 3.4. *Let $s \geq 1$. For $f \in \mathcal{L}_{QP}^2(\mathbb{R}^d)$ and $u \in \overline{\mathcal{H}}_{QP}^1(\mathbb{R}^d)$, with their parent functions $\mathcal{F} \in \mathcal{H}^s(\mathbb{T}^n), \mathcal{U} \in \mathcal{H}^{s+1}(\mathbb{T}^n)$, and under the regularity condition given by (3.11), there exists a constant C such that the following estimate holds*

$$\|u_T(\mathbf{x}) - u_N(\mathbf{x})\|_0 \leq CN^{-s} \|\mathcal{F}\|_{\mathcal{H}^s(\mathbb{T}^n)}.$$

Proof. Define $\psi(\mathbf{x}) = u(\mathbf{x}) - u_T(\mathbf{x})$ and $w_N(\mathbf{x}) = u_T(\mathbf{x}) - u_N(\mathbf{x})$. We can rewrite (3.9) as

$$\tilde{\mathcal{L}}w_N = (\tilde{\mathcal{L}} - \mathcal{L})u_T + \mathcal{L}\psi + f - f_I,$$

and have the subsequent inequality □

$$\begin{aligned} \gamma_0 \|w_N\|_1^2 &\leq (\tilde{\mathcal{L}}w_N, w_N) = ((\tilde{\mathcal{L}} - \mathcal{L})u_T, w_N) + (\mathcal{L}\psi, w_N) + (f - f_I, w_N) \\ &= T_1 + T_2 + T_3, \end{aligned}$$

using the ellipticity of $\tilde{\mathcal{L}}$. Next, we estimate the bounds for T_1, T_2, T_3 , respectively.

(i) For T_1 , we set $\phi = \alpha \nabla u_T \in \text{QP}(\mathbb{R}^d)$. Combining with (3.15), we obtain the inequality

$$T_1 = (\phi - I_N \phi, \nabla w_N) \leq CN^{-s} \|\mathcal{U}\|_{\mathcal{H}^{s+1}(\mathbb{T}^n)} \|\nabla w_N\|_0 \leq CN^{-s} \|\mathcal{U}\|_{\mathcal{H}^{s+1}(\mathbb{T}^n)} \|w_N\|_1.$$

(ii) For T_2 , we have

$$T_2 = (\alpha \nabla \psi, \nabla w_N) \leq C \|\nabla \psi\|_0 \|\nabla w_N\|_0 \leq CN^{-s} \|\mathcal{U}\|_{\mathcal{H}^{s+1}(\mathbb{T}^n)} \|w_N\|_1,$$

using the (3.14) from Lemma 3.3.

(iii) For T_3 , we have

$$T_3 = (f - f_I, w_N) \leq \|f - I_N f\|_0 \|w_N\|_0 \leq CN^{-s} \|\mathcal{F}\|_{\mathcal{H}^s(\mathbb{T}^n)} \|w_N\|_1.$$

Combining the upper bounds of T_1, T_2 and T_3 with the regularity condition (3.11), we obtain

$$\gamma_0 \|w_N\|_1^2 \leq CN^{-s} \|w_N\|_1 \|\mathcal{F}\|_{\mathcal{H}^s(\mathbb{T}^n)},$$

which implies

$$\|w_N\|_0 \leq \|w_N\|_1 \leq CN^{-s} \|\mathcal{F}\|_{\mathcal{H}^s(\mathbb{T}^n)}.$$

3.2.3. Proof of Theorem 3.1. Applying the triangle inequality, we have

$$\begin{aligned} \|u(\mathbf{x}) - u_N(\mathbf{x})\|_0 &\leq \|u(\mathbf{x}) - u_T(\mathbf{x})\|_0 + \|u_T(\mathbf{x}) - u_N(\mathbf{x})\|_0 \\ &:= \|\psi(\mathbf{x})\|_0 + \|w_N(\mathbf{x})\|_0. \end{aligned}$$

From the (3.12) provided in Lemma 3.2, we obtain

$$\|\psi\|_0 = \|u - u_T\|_0 \leq CN^{-s} |\mathcal{U}|_{\mathcal{H}^s(\mathbb{T}^n)},$$

As for the bound of $\|w_N\|_0$, we can conclude from the Lemma 3.4 that

$$\|w_N\|_0 = \|u_T - u_N\|_0 \leq CN^{-s} \|\mathcal{F}\|_{\mathcal{H}^s(\mathbb{T}^n)}.$$

Thus, we have the error estimate for the PM solving quasiperiodic elliptic equations

$$\begin{aligned} \|u - u_N\|_0 &\leq \|\psi\|_0 + \|w_N\|_0 \\ &\leq CN^{-s} |\mathcal{U}|_{\mathcal{H}^s(\mathbb{T}^n)} + CN^{-s} \|\mathcal{F}\|_{\mathcal{H}^s(\mathbb{T}^n)} \\ &\leq CN^{-s} \|\mathcal{U}\|_{\mathcal{H}^{s+1}(\mathbb{T}^n)} + CN^{-s} \|\mathcal{F}\|_{\mathcal{H}^s(\mathbb{T}^n)} \\ &\leq CN^{-s} \|\mathcal{F}\|_{\mathcal{H}^s(\mathbb{T}^n)}. \end{aligned}$$

4. Linear system solver. In this section, we first introduce the *compressed storage method* to leverage the multilevel block circulant structure of matrix A , reducing the memory storage requirement for Q . Moreover, we propose the *compressed PCG* (C-PCG) algorithm which incorporates our proposed diagonal preconditioner to accelerate the convergence rate.

4.1. Multi-level block circulant matrix. In this subsection, we analyze the structure of matrix $A \in \mathbb{C}^{D \times D}$ for general case $d \leq n$. The structure of A can be depicted by

$$\left\{ \begin{bmatrix} \tilde{\mathcal{A}}_{(\mathbf{0},0)} & \tilde{\mathcal{A}}_{(\mathbf{0},-1)} & \cdots & \tilde{\mathcal{A}}_{(\mathbf{0},1)} \\ \tilde{\mathcal{A}}_{(\mathbf{0},1)} & \tilde{\mathcal{A}}_{(\mathbf{0},0)} & \cdots & \tilde{\mathcal{A}}_{(\mathbf{0},2)} \\ \vdots & \vdots & \cdots & \vdots \\ \tilde{\mathcal{A}}_{(\mathbf{0},-1)} & \tilde{\mathcal{A}}_{(\mathbf{0},-2)} & \cdots & \tilde{\mathcal{A}}_{(\mathbf{0},0)} \end{bmatrix} \right\} \xrightarrow{A_{11}^{(1)}} \left\{ \begin{bmatrix} A_{11}^{(1)} & \begin{bmatrix} A_{12}^{(1)} \\ A_{11}^{(1)} \end{bmatrix} & \cdots & A_{1N}^{(1)} \\ \vdots & \vdots & \cdots & \vdots \\ A_{12}^{(1)} & A_{13}^{(1)} & \cdots & A_{11}^{(1)} \end{bmatrix} \right\} \xrightarrow{A_{11}^{(2)}} \cdots \xrightarrow{A} \left\{ \begin{bmatrix} A_{11}^{(n-1)} & \begin{bmatrix} A_{12}^{(n-1)} \\ A_{11}^{(n-1)} \end{bmatrix} & \cdots & A_{1N}^{(n-1)} \\ \vdots & \vdots & \cdots & \vdots \\ A_{12}^{(n-1)} & A_{13}^{(n-1)} & \cdots & A_{11}^{(n-1)} \end{bmatrix} \right\},$$

where $\mathbf{0}$ denotes an $(n-1)$ -dimensional zero vector. To obtain the matrix A , the initial step is computing the discrete Fourier coefficients of $\mathcal{A}(\mathbf{x})$, denoted as $\tilde{\mathcal{A}}$. Each row of $\tilde{\mathcal{A}}$ is then cyclically permuted to assemble the first-level block circulant matrix $A^{(1)}$. This matrix is further permuted to recursively construct the l -level block circulant matrix $A^{(l)}$ ($2 \leq l \leq n$), which consists of $N \times N$ blocks of $A^{(l-1)}$. As a result, A is referred to as an n -level *block circulant matrix* and can be conveniently expressed as follows

$$A = \sum_{\mathbf{k} \in K_N^n} \tilde{\mathcal{A}}_{\mathbf{k}} Z_N^{\mathbf{k}} = \sum_{k_1 \in K_N^1} \cdots \sum_{k_n \in K_N^1} \tilde{\mathcal{A}}_{(k_1, \dots, k_n)} Z_N^{k_1} \otimes \cdots \otimes Z_N^{k_n}, \quad \mathbf{k} = (k_1, \dots, k_n),$$

where

$$Z_N^k = \underbrace{\begin{bmatrix} 0 & \cdots & 1 & 0 & \cdots & 0 \\ \vdots & & & \ddots & & \vdots \\ \vdots & & & & \ddots & \vdots \\ 1 & 0 & & & & 1 \\ & \ddots & & & & \\ 0 & \cdots & 1 & \cdots & \cdots & 0 \end{bmatrix}}_{N \times N} \Bigg\}^{\overline{k}}$$

is the *cycling permutation matrix* and \otimes denotes the tensor product. It is worth mentioning that the N matrices $\{Z_N^{k_i}\}$, where $i = 1, \dots, N$, can be regarded as a canonical basis for the linear space of circulant matrices of order N . To enhance our intuitive grasp of matrix A , [Appendix D](#) provides an illustrative example of $d = 1$ and $n = 2$.

4.2. Compressed storage. In this subsection, we introduce the compressed storage method for the stiffness matrix $Q = A \circ W$. There are two steps involved in this method.

Step 1: Compression of A . As presented in the above subsection, the n -level block circulant matrix A is recursively generated from discrete Fourier coefficients $\tilde{\mathcal{A}}$. This enable us to store only $\tilde{\mathcal{A}}$ instead of the complete matrix A , to significantly reduce the memory usage. To achieve this, we utilize the relationship between the discrete Fourier coefficient $\tilde{\mathcal{A}}_{\mathbf{k}_A}$ ($\mathbf{k}_A = \mathbf{k}_V - \mathbf{k}_U$) and its

corresponding position (i, j) in A , as determined by (3.7). By assigning the value of $\tilde{\mathcal{A}}_{\mathbf{k}_A}$ to A_{ij} , we can effectively store D discrete Fourier coefficients $\tilde{\mathcal{A}}_{\mathbf{k}_A}$ along with $2D$ tensor indices $\mathbf{k}_V, \mathbf{k}_U$. This approach allows us to fully achieve compressed storage for matrix A and reduces memory requirements from $\mathcal{O}(D \times D)$ to $\mathcal{O}(D)$.

Step 2: Compression of W . The formula for W_{ij} is given by $W_{ij} = (\mathbf{P}\mathbf{k}_V)^T(\mathbf{P}\mathbf{k}_U)$. Since the indices i and j of W_{ij} align with those of A_{ij} , we can utilize the tensor indices \mathbf{k}_V and \mathbf{k}_U associated with A_{ij} to compute W_{ij} . This means that we can use the saved indices $\mathbf{k}_V, \mathbf{k}_U$ to compute W_{ij} without requiring additional memory for storing W .

The above steps can be summarized in Algorithm 4.1 as the “compressed storage method” for $Q = A \circ W$.

Algorithm 4.1 Compressed storage method for Q

Input: discrete Fourier coefficients $\tilde{\mathcal{A}}$, tensor indices $\mathbf{k}_V, \mathbf{k}_U$, projection matrix \mathbf{P}

Output: Q_{ij}

$$\mathbf{k}_V \xrightarrow{\mathcal{C}} i, \quad \mathbf{k}_U \xrightarrow{\mathcal{C}} j$$

$$\mathbf{k}_A = \mathbf{k}_V - \mathbf{k}_U$$

$$A_{ij} = \tilde{\mathcal{A}}_{\mathbf{k}_A}$$

$$W_{ij} = (\mathbf{P}\mathbf{k}_V)^T(\mathbf{P}\mathbf{k}_U)$$

$$Q_{ij} = A_{ij}W_{ij}$$

PROPOSITION 4.1. *The memory requirement for the compressed storage method is $\mathcal{O}(D)$, resulting in a memory reduction of order $\mathcal{O}(D)$.*

Furthermore, in preparation for the subsequent improved iterative solver, we introduce the set \mathcal{Z} that comprises all non-zero elements of Q ,

$$\mathcal{Z} = \{Q_{ij} : Q_{ij} \neq 0, i, j = 1, \dots, D\}.$$

We denote the compressed format of Q as $\tilde{Q} = (i, j, Q_{ij})_{Q_{ij} \in \mathcal{Z}}$. Going forward, all matrix-vector multiplications involving Q will be replaced by \tilde{Q} . This technique is referred to as *compressed matrix-vector multiplication*.

4.3. Preconditioner and C-PCG. In this subsection, we propose an efficient iterative approach based on conjugate gradient (CG) method to solve linear system (3.8). As subsection 4.3 shows, the linear system becomes ill-conditioned with an increase of discrete points. Therefore, it is crucial to design efficient preconditioners to reduce the condition number. Here, we propose a diagonal preconditioner by the following matrix minimization problem (4.1)

$$(4.1) \quad M = \underset{\mathcal{D} \in \mathcal{D}(D)}{\operatorname{argmin}} \|\mathbf{Q}\mathcal{D} - \mathbf{I}_D\|_F.$$

The optimization problem can be solved analytically.

THEOREM 4.2. *The solution of (4.1) is*

$$(4.2) \quad M = \operatorname{diag}(q_{11}/\|\mathbf{Q}\mathbf{e}_1\|_2^2, \dots, q_{DD}/\|\mathbf{Q}\mathbf{e}_D\|_2^2).$$

Proof. Given matrices $Q = (q_{ij}) \in \mathbb{C}^{D \times D}$ and $M = \text{diag}(m_{11}, \dots, m_{DD}) \in \mathcal{D}(D)$, we can compute $QM - I_D$ as follows

$$QM - I_D = \begin{bmatrix} q_{11}m_{11} - 1 & q_{12}m_{22} & \cdots & q_{1D}m_{DD} \\ q_{21}m_{11} & q_{22}m_{22} - 1 & \cdots & q_{2D}m_{DD} \\ \vdots & \vdots & \ddots & \vdots \\ q_{D1}m_{11} & q_{D2}m_{22} & \cdots & q_{DD}m_{DD} - 1 \end{bmatrix}.$$

Hence

$$\begin{aligned} \|QM - I_D\|_F^2 &= (q_{11}m_{11} - 1)^2 + (q_{12}m_{22})^2 + \cdots + (q_{1D}m_{DD})^2 \\ &\quad + (q_{21}m_{11})^2 + (q_{22}m_{22} - 1)^2 + \cdots + (q_{2D}m_{DD})^2 \\ &\quad \vdots \\ &\quad + (q_{D1}m_{11})^2 + (q_{D2}m_{22})^2 + \cdots + (q_{DD}m_{DD} - 1)^2. \end{aligned}$$

The j -th column summation $S_j = (q_{1j}m_{jj})^2 + \cdots + (q_{jj}m_{jj} - 1)^2 + \cdots + (q_{Dj}m_{jj})^2 = (\sum_{i=1}^D q_{ij}^2)m_{jj}^2 - 2q_{jj}m_{jj} + 1$. Obviously, S_j is a quadratic function with respect to m_{jj} and it attains its minimum if and only if $m_{jj} = q_{jj}/(\sum_{i=1}^D q_{ij}^2) = q_{jj}/\|Q\mathbf{e}_j\|_2^2$. \square

PROPOSITION 4.3. *Suppose $\tilde{\mathcal{A}}$ contains g non-zero elements. In this case, each row (or column) of Q consists of $\mathcal{O}(g)$ non-zero elements. Therefore, the computational complexity for constructing M amounts to $\mathcal{O}(gD)$.*

To demonstrate the effectiveness of the diagonal preconditioner M , we perform a numerical test with $d = 1, n = 2$. The implementation of this case can be found in [Subsection 5.1.1](#). As illustrated in [Subsection 4.3](#), the condition number of Q exhibits a substantial increase as N grows. However, after applying the preconditioner M , the condition number undergoes a significant reduction and stabilizes within a very narrow range.

N	4	8	16	32	64	128
Q	1.77e+01	7.31e+01	2.97e+02	1.19e+03	4.81e+03	1.93e+04
QM	2.44	2.48	2.44	2.49	2.49	2.48

Table 1: Condition number of Q and preconditioned system QM .

Moreover, we use the compressed matrix-vector multiplication to accelerate the iteration process further in iterative schemes like PCG. This improved PCG method, referred to as compressed PCG (C-PCG) method, is outlined in [Algorithm 4.2](#).

Algorithm 4.2 C-PCG method

Given initial guess vector U_0 and compute the residual $r_0 = F - \tilde{Q}U_0$
 Solve residual equation $Mz_0 = r_0$, set $h_0 = z_0$
for $j = 0, 1, \dots$, until convergence **do**
 $\alpha_j = \frac{(r_j, z_j)}{\tilde{Q}h_j, h_j}$
 $U_{j+1} = U_j + \alpha_j h_j$
 $r_{j+1} = r_j - \alpha_j \tilde{Q}h_j$
 Solve $Mz_{j+1} = r_{j+1}$
 $\beta_j = \frac{(r_{j+1}, z_{j+1})}{r_j, z_j}$
 $h_{j+1} = z_{j+1} + \beta_j h_j$
end for

REMARK 4.1. Compared to standard PCG, C-PCG utilizes the compressed form \tilde{Q} instead of Q to enhance matrix-vector multiplication. In terms of computational complexity, the C-PCG method reduces it from $\mathcal{O}(D \times D)$ to $\mathcal{O}(gD)$, which is equivalent to the costs of compressed matrix-vector multiplication. Moreover, it is worth emphasizing that we can substitute the PCG method with other iterative approaches if desired.

5. Numerical experiments. In this section, we present two classes of numerical experiments to demonstrate the performance of our algorithm. Firstly, we employ the PM to solve the quasiperiodic elliptic equation (2.8) and compare its efficiency with the PAM. We also compare the performance of PCG and C-PCG in solving the linear system discretized by PM. Consequently, we focus on the quasiperiodic homogenization problem and demonstrate the accuracy and efficiency of our algorithm in calculating the homogenized coefficients. These experiments are conducted using MATLAB R2017b on a laptop computer equipped with an Intel Core 2.50GHz CPU and 4GB RAM. The computational time, measured in seconds(s), is referred to as CPU time.

5.1. Quasiperiodic elliptic equations. In this subsection, we present several examples to demonstrate the effectiveness of the proposed algorithm. In the first example, the spectral points of the elliptic coefficient and the solution are two separated incommensurate frequencies, namely 1 and $\sqrt{2}$. We begin with implementing the PM to solve the quasiperiodic elliptic equation (2.8) using the C-PCG method. Our numerical experiments involve comparing the CPU time and memory usage between standard PCG and C-PCG to demonstrate the high efficiency of C-PCG. Furthermore, we give a comparative analysis of the accuracy and efficiency of PM against the PAM, emphasizing the advantages of PM in solving quasiperiodic elliptic equations, particularly in avoiding the Diophantine approximation error. The second example is more complex, its spectral point set of solution consists of linear combinations of 1 and $\sqrt{2}$. More examples can be found in Appendix G.

In the following, we denote the numerical solutions as u_N , where N represents the number of discrete points in each dimension. We use the $\mathcal{L}_{QP}^2(\mathbb{R}^d)$ -norm to measure the numerical error $e_N = \|u_N - u\|_{\mathcal{L}_{QP}^2(\mathbb{R}^d)}$, where u is the exact solution of (2.8). The error order is calculated by $\kappa = \frac{\ln(e_{N_1}/e_{N_2})}{\ln(N_1/N_2)}$.

5.1.1. Two separated incommensurate frequencies. In the first test, we aim to demonstrate the accuracy and efficiency of the PM together with C-PCG iterative solver. For the quasiperiodic elliptic equation (2.8), we choose the coefficient $\alpha_1(x) = \cos(2\pi x) + \cos(2\pi\sqrt{2}x) + 6$ and the exact solution $u_1(x) = \sin(2\pi x) + \sin(2\pi\sqrt{2}x)$.

C-PCG vs. PCG in PM scheme. Within the PM framework, we compare the efficiency, memory usage, and condition number of PCG and C-PCG. Subsection 4.3 has presented the condition number of Q and QM , and shown that our proposed diagonal preconditioner M is very efficient. Table 2 compares the efficiency of PCG with C-PCG. We can find that the C-PCG can significantly reduce the CPU time compared with the PCG. As N grows, the reduction in CPU time diminishes rapidly. Meanwhile, the C-PCG achieves significant memory savings, as shown in Table 3. We denote the memory usage (in units of Gb) of PCG and C-PCG as M_{PCG} and $M_{\text{C-PCG}}$, respectively. Visually, as depicted in Figure 1, the ratio $r = M_{\text{PCG}}/M_{\text{C-PCG}}$ is approximately $\mathcal{O}(D)$. For example, when $N = 32$, it is apparent that memory requirement of PCG is $1025 \approx 32^2$ times larger than that of C-PCG.

N	4	8	16	32	64	128
CPU time(PCG)	0.05	0.78	9.63	135.60	-	-
CPU time(C-PCG)	0.02	0.07	0.27	1.04	4.89	17.32
Iteration(PCG)	13	19	19	19	-	-
Iteration(C-PCG)	13	19	19	19	19	19
$e_N(\text{PCG})$	6.24e-02	3.02e-16	5.09e-16	5.66e-16	-	-
$e_N(\text{C-PCG})$	6.24e-02	3.02e-16	5.10e-16	5.66e-16	4.35e-16	3.62e-16

Table 2: Efficiency comparison of PCG and C-PCG when solving (2.8) with $(\alpha_1(x), u_1(x))$ in PM (Data for $N \geq 64$ with PCG is not available due to insufficient memory).

N	4	8	16	32	64	128
M_{PCG}	1.00e-03	1.60e-02	2.50e-01	4.00e+00	6.40e+01	1.02e+03
$M_{\text{C-PCG}}$	6.11e-05	2.44e-04	9.77e-04	3.90e-03	1.56e-02	6.25e-02

Table 3: Comparison between M_{PCG} and $M_{\text{C-PCG}}$.

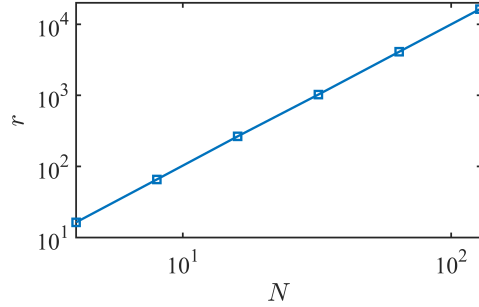


Fig. 1: The ratio $r = M_{\text{PCG}}/M_{\text{C-PCG}}$ vs. N in log-log scale.

PM vs. PAM. We provide a comprehensive comparison between the PM and the PAM in solving (2.8). The implementation of PAM is provided in Appendix E. We use periodic functions

$\alpha_{1p}(x) = \cos(2\pi x) + \cos(2\pi([\sqrt{2}L]/L)x) + 6$ with varying L , representing the length of the computational area, to approximate the quasiperiodic coefficient $\alpha_1(x) = \cos(2\pi x) + \cos(2\pi\sqrt{2}x) + 6$. In PAM, we choose $E = L \times N$ discrete points to ensure enough numerical accuracy of discretizing (2.8) with $N = 16$. For convenience, we continue to use e_N to denote the numerical error of PAM. We only present the results when $L = 2, 5, 12, 29, 70, 169, 408$ for PAM. Figure 2 shows the Diophantine approximation error $|L\sqrt{2} - [L\sqrt{2}]|$ with respect to L , intending to explain why these particular L are chosen for approximation. Our tests not only involve computing the numerical error e_N , but also giving a qualitative relationship between the numerical error and the Diophantine approximation error, as presented in Table 4. As we can see, e_N is mainly controlled by the Diophantine approximation error. Furthermore, we fix L and gradually increase $N = 2^k, k \in \mathbb{N}^+$. In Table 5, we observe that PAM fails to achieve improved accuracy even with a significantly higher number of discrete points. The numerical error stagnates once N exceeds a certain value. More theoretical results on function approximation theory in the context of PAM can refer to [14].

L	2	5	12	29	70	169	408
$[\sqrt{2}L]/L$	3/2	7/5	17/12	41/29	99/70	239/169	577/408
$ L\sqrt{2} - [L\sqrt{2}] $	1.72e-01	7.11e-02	2.94e-02	1.22e-02	5.10e-03	2.10e-03	8.67e-04
e_N	2.12e-01	9.18e-02	3.77e-02	1.56e-02	6.50e-03	2.70e-03	1.10e-03

Table 4: Numerical error of PAM in solving (2.8) with $\alpha_{1p}(x)$ and corresponding Diophantine approximation error against L .

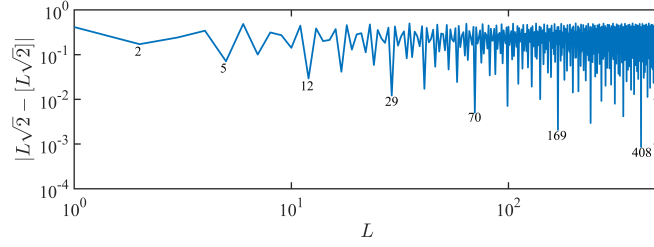


Fig. 2: Diophantine approximation error of $\sqrt{2}$.

e_N	$k = 2$	$k = 3$	$k = 4$	$k = 5$	$k = 6$
$L = 2$	5.55e-01	2.17e-01	2.12e-01	2.11e-01	2.11e-01
$L = 5$	5.41e-01	9.17e-02	9.18e-02	9.18e-02	9.18e-02
$L = 12$	5.27e-01	3.77e-02	3.77e-02	3.77e-02	3.77e-02
$L = 29$	5.07e-01	1.56e-02	1.56e-02	1.56e-02	1.56e-02

Table 5: Numerical error with variable $E = L \times 2^k$ for different L in PAM.

We then compare the efficiency of PM and PAM. Table 6 presents the accuracy achieved by these two methods, along with their required CPU time. Moreover, Figure 3 provides a visual representation of the trade-off between cost (CPU time) and accuracy. It is evident that PM avoids

the impact of Diophantine approximation errors and achieves machine precision in a short amount of time. In contrast, PAM, even with much larger CPU time, only achieves relatively low accuracy, which is dependent on the Diophantine approximation error.

	N	4	8	16
e_N	PM	6.24e-02	3.02e-16	5.10e-16
	PAM($L = 70$)	5.02e-01	6.50e-03	6.50e-03
	PAM($L = 169$)	4.98e-01	2.70e-03	2.70e-03
	PAM($L = 408$)	3.97e-01	1.10e-03	1.10e-03
CPU time	PM	1.77e-02	7.08e-02	1.73e-01
	PAM($L = 70$)	7.23e-02	2.53e-01	6.52e-01
	PAM($L = 169$)	1.42e-01	5.78e-01	1.53
	PAM($L = 408$)	2.56e-01	1.60	5.30

Table 6: Performance comparison between PM and PAM in solving (2.8) with $\alpha_1(x)$.

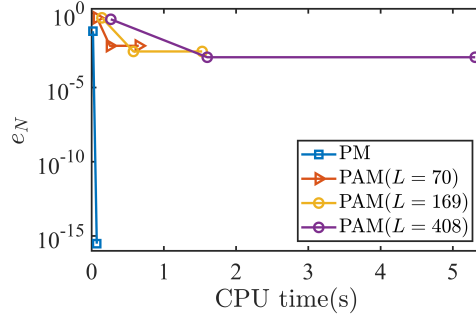


Fig. 3: Cost-Accuracy trade-off of PM and PAM ($L = 70, 169, 408$) in solving (2.8) with $\alpha_1(x)$ respectively.

Convergence of solution without an exact solution example. We provide an example without closed-form solution to validate the correctness of our algorithm. We select $\alpha_1(x)$ as the coefficient and $f(x) = \sin(2\pi x) + \sin(2\pi\sqrt{2}x)$ as the right-hand-side. The reference solution is given by PM under $N = 64$. Figure 4 shows that the PM solution u_N spectral accuracy converges to the reference solution as N increases. The numerical error e_N reaches machine precision when $N = 32$.

5.1.2. Combination of two incommensurate frequencies. To demonstrate the spectral accuracy of the PM and highlight the high efficiency of C-PCG further, we design a more complex example where the spectral points of solution u are formed by a linear combination of 1 and $\sqrt{2}$. We adopt the coefficient $\alpha_1(x)$ and the exact solution $u_2(x)$ in the following form

$$u_2(x) = \sum_{\lambda \in \Lambda_K} \tilde{u}_\lambda e^{i2\pi\lambda x}, \quad \tilde{u}_\lambda = e^{-(|k_1|+|k_2|)}, \quad \Lambda_K = \left\{ \lambda = k_1 + k_2\sqrt{2} : -32 \leq k_1, k_2 < 32 \right\}.$$

Similar to the first test, we evaluate the performance of PCG and C-PCG by comparing with their numerical error and CPU time. Subsection 5.1.2 once again demonstrates that C-PCG solves

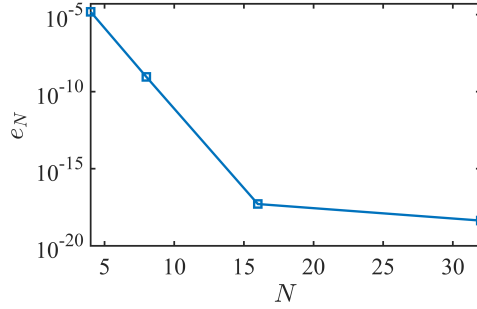


Fig. 4: Numerical error for the PM solution of (2.8) without closed-form solution.

(2.8) more efficiently. Furthermore, thanks to the memory savings of C-PCG, we observe the exponential decay of e_N to machine precision, sufficiently covering all non-zero values of \tilde{u}_λ . Additionally, the error order κ continues to increase with N . These numerical results show that the PM can achieve spectral accuracy in solving quasiperiodic elliptic equations, which aligns with our convergence results.

N	4	8	16	32	64	128
e_N (PCG)	2.73	2.02e-01	5.72e-04	8.32e-08	-	-
e_N (C-PCG)	2.73	2.02e-01	5.72e-04	8.32e-08	2.42e-15	2.46e-15
κ	-	3.75	8.46	12.75	18.75	-
CPU time(PCG)	2.80e-03	4.26e-02	7.16e-01	1.13e+01	-	-
CPU time(C-PCG)	7.08e-04	3.01e-03	1.12e-02	4.84e-02	1.57e-01	5.37e-01
Iteration (PCG)	14	19	18	18	-	-
Iteration (C-PCG)	14	19	18	18	18	18

Table 7: Efficiency comparison of PCG and C-PCG when solving (2.8) with $(\alpha_1(x), u_2(x))$ in PM (Data for $N \geq 64$ with PCG is not available due to insufficient memory).

5.2. Quasiperiodic homogenization. In this subsection, we apply PM to quasiperiodic homogenization. Within the framework of classical two-scale homogenization, we consider the coefficient $A(\mathbf{x}/\varepsilon)$, where $\varepsilon \ll 1$. The corresponding solution is denoted as u_ε , and as $\varepsilon \rightarrow 0$, we expect the convergence of u_ε to u^* , which represents the solution of an elliptic equation with a homogenized coefficient A^* . Alternatively, we can perform a scaling transformation of the variable $\mathbf{x}/\varepsilon \rightarrow \mathbf{x}$, which allows us to transform the domain from a bounded region to the entire space. When $A(\cdot)$ is periodic, it is possible to construct the corrector equation on the periodic cell. However, when $A(\cdot)$ is quasiperiodic, the corresponding quasiperiodic corrector equation is posed on the whole space

$$(5.1) \quad -\operatorname{div}(A_{\text{q-per}}(\mathbf{x})(\mathbf{p} + \nabla u_{\mathbf{p}}(\mathbf{x}))) = 0, \quad \mathbf{x} \in \mathbb{R}^d,$$

where the scalar-valued coefficient matrix $A_{\text{q-per}}(\mathbf{x})$ is uniformly elliptic, and $\mathbf{p} \in \mathbb{R}^d$ is an arbitrary vector. According to the homogenization theory [5], A^* can be computed by the following formula

$$(5.2) \quad A_{ij}^* = \mathcal{M} \{ \mathbf{e}_i^T A_{\text{q-per}}(\mathbf{x})(\mathbf{e}_j + \nabla u_{\mathbf{e}_j}(\mathbf{x})) \}.$$

The numerical challenge lies in accurately solving the quasiperiodic corrector equation (5.1). Our developed algorithm addresses this crucial issue by leveraging the periodic structure in the high dimensions, thereby enhances the overall efficiency and accuracy. To demonstrate the effectiveness of our approach, we provide a numerical example in the following. Further details about the solution procedure can be found in [Appendix F](#).

We consider the corrector equation (5.1) with

$$(5.3) \quad A_{\text{q-per}}(x_1, x_2) = \begin{pmatrix} 4 + \cos(2\pi(x_1 + x_2)) & 0 \\ + \cos(2\pi\sqrt{2}(x_1 + x_2)) & 6 + \sin^2(2\pi x_1) \\ 0 & + \sin^2(2\pi\sqrt{2}x_1) \end{pmatrix},$$

which also appears in [2]. The corresponding projection matrix is

$$\mathbf{P} = 2\pi \cdot \begin{pmatrix} 1 & \sqrt{2} & 1 & \sqrt{2} \\ 1 & \sqrt{2} & 0 & 0 \end{pmatrix}.$$

We calculate a reference approximation of A^* using PM discretization with $N = 18$, denoted as A_{ref}^* . The formula (5.2) can be expressed in terms of (F.6)-(F.9). Then, we compute the numerical homogenized coefficients $A_{11,N}^*$ and $A_{22,N}^*$, and record the corresponding numerical errors $e_{11,N}^* = |A_{11,N}^* - A_{11,\text{ref}}^*|$ and $e_{22,N}^* = |A_{22,N}^* - A_{22,\text{ref}}^*|$ in [Table 8](#). These results demonstrate that $e_{11,N}^*$ and $e_{22,N}^*$ spectral accuracy converge as N increases, with A_{ref}^* already possessing a minimum accuracy of 10 digits.

N	2	4	6	8
$e_{11,N}^*$	9.19e-02	1.60e-03	3.18e-05	7.23e-07
$e_{22,N}^*$	9.92e-01	8.11e-03	1.87e-04	4.37e-06
N	10	12	14	16
$e_{11,N}^*$	1.77e-08	4.56e-10	1.21e-11	3.17e-13
$e_{22,N}^*$	1.03e-07	2.45e-09	5.89e-11	1.45e-12

Table 8: Numerical errors for homogenized coefficients A_{11}^* and A_{22}^* calculated by the C-PCG method with PM discretization.

For comparison, we also compute A_{11}^* by PAM. To approximate (5.3), we take

$$(5.4) \quad A_{\text{per}}(x_1, x_2) = \begin{pmatrix} 4 + \cos(2\pi(x_1 + x_2)) + & 0 \\ \cos(2\pi([\sqrt{2}L]/L)(x_1 + x_2)) & 6 + \sin^2(2\pi x_1) + \\ 0 & \sin^2(2\pi([\sqrt{2}L]/L)x_1) \end{pmatrix}$$

by varying computational area $[0, L]^2$. The homogenized coefficients in the periodic case reads

$$(5.5) \quad A_{ij}^* = \frac{1}{L^2} \int_{[0,L]^2} \mathbf{e}_i^T A_{\text{per}}(\mathbf{x})(\mathbf{e}_j + \nabla u_{\mathbf{e}_j}(\mathbf{x})) d\mathbf{x}.$$

In [Figure 5\(a\)](#), the orange line represents $A_{11,\text{ref}}^*$ calculated by PM, serving as the reference solution. The blue line corresponds to the approximation results obtained by varying L in PAM, denoted as

$A_{11,L}^*$. The approximation values $A_{11,L}^*$ and the corresponding numerical errors $e_{11,L}^* = |A_{11,L}^* - A_{11,\text{ref}}^*|$ are displayed in Figure 5(a) and Figure 5(b), respectively. In Figure 5(a), we notice a slow convergence of PAM in computing the quasiperiodic homogenized coefficient. Furthermore, Figure 5(b) shows that $e_{11,L}^*$ does not consistently decrease as L increases, mainly because of the unavoidable impact of the Diophantine approximation error.

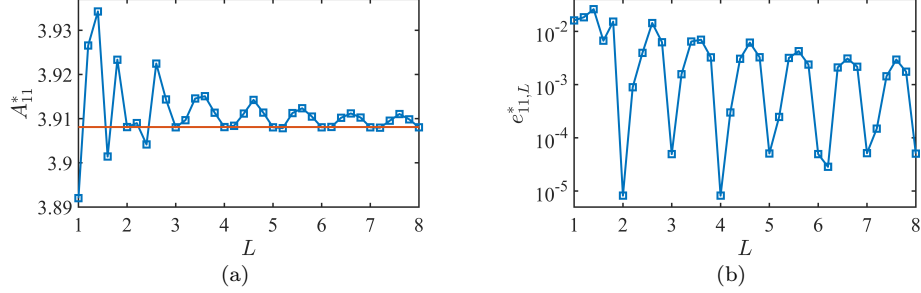


Fig. 5: Figure 5(a): Approximation values of A_{11}^* calculated by PM (orange line) and PAM (blue line) ; Figure 5(b): Numerical error $e_{11,L}^*$ of PAM in calculating A_{11}^* vs. L .

In the following, we compare the efficiency between PM and PAM for quasiperiodic homogenization. Table 9 showcases the error $e_{11,N}^*$ computed by PM and PAM, along with the corresponding CPU time. The data indicates that the error in solving the homogenization problem using PM can quickly reach high precision within a very short time, whereas the accuracy of PAM stabilizes at a lower level. Furthermore, Figure 6 visualizes the cost-accuracy trade-off of PM and PAM, clearly demonstrating the high efficiency of the PM.

	N	4	8	16
$e_{11,N}^*$	PM	1.51e-03	7.07e-07	3.18e-13
	PAM($L = 29$)	1.56e-03	3.46e-04	3.4e-04
	PAM($L = 70$)	1.07e-03	1.98e-04	1.98e-04
CPU time	PM	1.63e-02	5.64e-01	2.89
	PAM($L = 29$)	1.04e-01	1.13	6.61
	PAM($L = 70$)	6.27e-01	7.34	42.73

Table 9: Performance comparison between PM and PAM in computing A_{11}^* .

6. Conclusion and outlook. This paper focuses on the development of an efficient algorithm for solving quasiperiodic elliptic equations, and in particular, its application in quasiperiodic homogenization. We utilize the PM to discretize the quasiperiodic elliptic equation and obtain a linear system through the tensor-vector-index conversion. Meanwhile, we provide a rigorous convergence analysis to demonstrate that our algorithm achieves spectral accuracy. To reduce computational costs, we propose a compressed storage method and employ the C-PCG iteration with a diagonal preconditioner. Memory analysis and complexity analysis are provided to assess the algorithm's efficiency. We apply our algorithm to solve quasiperiodic elliptic equations and compute the homogenized coefficients of a multiscale quasiperiodic PDE. Numerical results demonstrate the

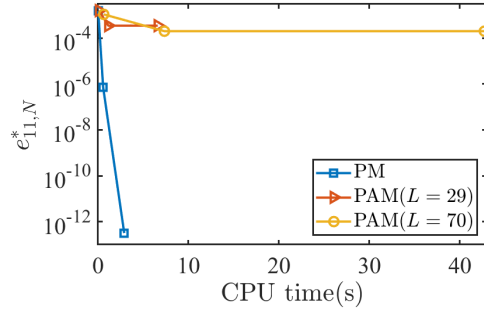


Fig. 6: Cost-Accuracy trade-off of PM and PAM ($L = 29, 70$) in computing A_{11}^* , respectively.

effectiveness of our algorithm, showing it successfully avoids the Diophantine approximation error and further validates the theoretical results.

In the future, we plan to perform more comprehensive investigations in several areas. Firstly, we aim to extend our method to handle other types of PDEs with quasiperiodic coefficients, including parabolic equations and wave equations. Secondly, we intend to provide a thorough convergence analysis of the PM for solving quasiperiodic PDEs. The analysis will offer a deeper understanding of the method's theoretical properties. Lastly, we plan to develop the PM to address nonlinear homogenization problems, which will involve tackling additional challenges and exploring novel computational strategies. All these projects will not only enhance the theoretical foundation of our method but also contribute to its practical application in quasiperiodic PDEs.

REFERENCES

- [1] D. Braess, *Finite elements: Theory, fast solvers, and applications in solid mechanics*, Cambridge University Press, 2001.
- [2] X. Blanc and C. Le Bris, *Improving on computation of homogenized coefficients in the periodic and quasiperiodic settings*, Networks and Heterogeneous Media, **5**(2010), 1–29.
- [3] A. Bensoussan, J. L. Lions, and G. Papanicolaou, *Asymptotic analysis for periodic structures*, vol.374, American Mathematical Soc., 2011.
- [4] K. Barkan, M. Engel and R. Lifshitz, *Controlled self-assembly of periodic and aperiodic cluster crystals*, Physical review letters, **113**(2014), 098304.
- [5] X. Blanc and C. Le Bris, *Homogenization theory for multiscale problems: an introduction*, vol.21, Springer Nature, 2023.
- [6] Y. Cao, V. Fatemi, S. Fang, K. Watanabe, T. Taniguchi, E. Kaxiras, and P. Jarillo-Herrero, *Unconventional superconductivity in magic-angle graphene superlattices*, Nature, **556**(2010), 43–50.
- [7] D. Cao, J. Shen and J. Xu, *Computing interface with quasiperiodicity*, Journal of Computational Physics, **424**(2021), 109863.
- [8] Z. Gao, Z. Xu, Z. Yang and F. Ye, *Pythagoras superposition principle for localized eigenstates of 2D Moiré lattices*, Physical Review A, **108**(2023), 013513.
- [9] K. Jiang and P. Zhang, *Numerical methods for quasicrystals*, Journal of Computational Physics, **256**(2014), 428–440.
- [10] K. Jiang, J. Tong, P. Zhang and A. C. Shi, *Stability of two-dimensional soft quasicrystals in systems with two length scales*, Physical Review E, **92**(2015), 042159.
- [11] K. Jiang and P. Zhang, *Numerical mathematics of quasicrystals*, Proceedings of the International Congress of Mathematicians: Rio de Janeiro (2018), 3591–3609.
- [12] X. Li, and K. Jiang, *Numerical simulation for quasiperiodic quantum dynamical systems*, Journal on Numerica

- Methods and Computer Applications, **42**(2021), 3.
- [13] K. Jiang, W. Si and J. Xu, *Tilt grain boundaries of hexagonal structures: a spectral viewpoint*, SIAM Journal on Applied Mathematics, **82**(2022), 1267–1286.
 - [14] K. Jiang, S. Li and P. Zhang, *On the approximation of quasiperiodic functions with Diophantine frequencies by periodic functions*, arXiv:2304.04334, (2023).
 - [15] K. Jiang, S. Li and J. Zhang, *High-accuracy numerical methods and convergence analysis for Schrödinger equation with incommensurate potentials*, Journal of Scientific Computing, **101**(2024), 18.
 - [16] K. Jiang, S. Li and P. Zhang, *Numerical methods and analysis of computing quasiperiodic systems*, SIAM Journal on Numerical Analysis, **62**(2024), 353–375.
 - [17] S. M. Kozlov, *Averaging differential operators with almost periodic, rapidly oscillating coefficients*, Mathematics of the USSR-Sbornik, **35**(1979), 481.
 - [18] D. Levine and P. J. Steinhardt, *Quasicrystals: a new class of ordered structures*, Physical Review Letters, **53**(1984), 2477.
 - [19] G. Nguetseng, *Homogenization structures and applications I*, Zeitschrift für Analysis und ihre Anwendungen, **22**(2003), 73–108.
 - [20] H. Poincaré, *On the problem of three bodies and equations of dynamics*, Acta Mathematica, **13**(1890), A3–A270.
 - [21] R. Penrose, *The role of aesthetics in pure and applied mathematical research*, Bull. Inst. Math. Appl., **10**(1974), 266–271.
 - [22] D. Shechtman, I. Blech and D. Gratias, *Metallic phase with long-range orientational order and no translational symmetry*, Physical review letters, **53**(1984), 1951.
 - [23] A. P. Sutton, *Irrational interfaces*, Progress in Materials Science, **36**(1992), 167–202.
 - [24] P. Walters, *An introduction to ergodic theory*, vol. 79, Springer Science & Business Media, 2000.
 - [25] C. Wang, F. Liu and H. Huang, *Effective model for fractional topological corner modes in quasicrystals*, Physical Review Letters, **129**(2022), 056403.
 - [26] V. V. Zhikov, *Averaging of functionals of the calculus of variations and elasticity theory*, Mathematics of the USSR-Izvestiya, **29**(1987), 33.

Appendix A. Equivalent modulus theorem.

LEMMA A.1 (Equivalent modulus theorem [1]). *If bounded linear functionals L_1, L_2, \dots, L_K on $\mathcal{H}_{QP}^s(\mathbb{R}^d)$, $s \in \mathbb{N}^+$ is not simultaneously zero for any non-zero polynomial of degree $\leq s-1$, then for all $u \in \mathcal{H}_{QP}^s(\mathbb{R}^d)$, modules $\|u\|_s$ and $|u|_s + \sum_{i=1}^K |L_i(u)|$ are equivalent, that is, there are constants $c_1, c_2 > 0$ such that the following inequality holds*

$$(A.1) \quad c_1 \left(|u|_s + \sum_{i=1}^K |L_i(u)| \right) \leq \|u\|_s \leq c_2 \left(|u|_s + \sum_{i=1}^K |L_i(u)| \right).$$

Proof. We start from the left inequality. Since $L_i, i = 1, 2, \dots, K$ are bounded linear functionals in $\mathcal{H}_{QP}^s(\mathbb{R}^d)$, then we have

$$|L_i(u)| \leq \alpha_i \|u\|_s, \quad i = 1, 2, \dots, K.$$

Combining with

$$|u|_s \leq \|u\|_s,$$

we have

$$|u|_s + \sum_{i=1}^K |L_i(u)| \leq \left(1 + \sum_{i=1}^K \alpha_i \right) \|u\|_s.$$

The conclusion holds by setting $c_1 = \left(1 + \sum_{i=1}^K \alpha_i \right)^{-1}$.

To establish the right inequality, we utilize a proof by contradiction. If it is not true, then for any $n \in \mathbb{N}^+$, there must exist $v_n \in \mathcal{H}_{QP}^s(\mathbb{R}^d)$ such that

$$\|v_n\|_s > n \left(|v_n|_s + \sum_{i=1}^K |L_i(v_n)| \right).$$

Let $u_n = v_n / \|v_n\|_s$, then u_n satisfies

$$(A.2) \quad \|u_n\|_s = 1,$$

and

$$(A.3) \quad |u_n|_s + \sum_{i=1}^K |L_i(u_n)| < \frac{1}{n}.$$

Firstly, $\{u_n\}$ is a bounded sequence in $\mathcal{H}_{QP}^s(\mathbb{R}^d)$. We know that $\mathcal{H}_{QP}^s(\mathbb{R}^d) \hookrightarrow \mathcal{H}_{QP}^0(\mathbb{R}^d)$, therefore, there must be a subsequence (still denoted as u_n) that converges in $\mathcal{H}_{QP}^0(\mathbb{R}^d)$, then we have

$$\|u_n - u_m\|_0 \rightarrow 0, \quad n, m \rightarrow \infty.$$

Using (A.3), it holds that

$$|u_n - u_m|_s \leq |u_n|_s + |u_m|_s < \frac{1}{n} + \frac{1}{m} \rightarrow 0, \quad n, m \rightarrow \infty,$$

then

$$\|u_n - u_m\|_s = (\|u_n - u_m\|_0^2 + |u_n - u_m|_s^2)^{1/2} \rightarrow 0, \quad n, m \rightarrow \infty.$$

Consequently, $\{u_n\}$ is a Cauchy sequence in $\mathcal{H}_{QP}^s(\mathbb{R}^d)$ and there exists a $u \in \mathcal{H}_{QP}^s(\mathbb{R}^d)$ such that

$$\|u_n - u\|_s \rightarrow 0, \quad |u_n - u|_s \rightarrow 0, \quad n \rightarrow \infty.$$

Taking the limit on both sides of (A.2), we have

$$\|u\|_s = 1,$$

i.e., $u \neq 0$. Taking the limit on both sides of (A.3), we have

$$|u|_s = 0, \quad \sum_{i=1}^K |L_i(u)| = 0.$$

That is, for all $|p| = s$, we have $D^p u = 0$. Then we conclude that u is a polynomial of degree $s - 1$ such that $|L_i(u)| = 0$ for $i = 1, 2, \dots, K$. However, this contradicts the assumption. Therefore, we complete the proof. \square

Appendix B. Poincaré's inequality.

LEMMA B.1 (Poincaré's inequality). *For all $u \in \overline{\mathcal{H}}_{QP}^1(\mathbb{R}^d)$, we have*

$$(B.1) \quad \|u\|_1 \leq c_2 |u|_1.$$

Proof. Applying Lemma A.1 with $s = 1$ and $L(u) = \int u d\mathbf{x}$, we have

$$(B.2) \quad \begin{aligned} |L(u)| &= \left| \int u d\mathbf{x} \right| \leq \left(\int 1^2 d\mathbf{x} \right)^{1/2} \left(\int u^2 d\mathbf{x} \right)^{1/2} \\ &= \|u\|_0 \leq \|u\|_1 \end{aligned}$$

by using the Hölder's inequality. Therefore, $L(\cdot)$ is a bounded linear functional on $\mathcal{H}_{QP}^1(\mathbb{R}^d)$. And for any non-zero constant b , we have

$$L(b) = \int b d\mathbf{x} = b \int 1 d\mathbf{x} = b \neq 0.$$

By Lemma A.1, we have

$$\|u\|_1 \leq c_2 \left(|u|_1 + \int u d\mathbf{x} \right).$$

Moreover, $u \in \overline{\mathcal{H}}_{QP}^1(\mathbb{R}^d)$ implies $\int u d\mathbf{x} = 0$, then we complete the proof. \square

Appendix C. Wellposedness of discrete quasiperiodic elliptic problem.

THEOREM C.1. *The discrete variational formulation (3.1) has a unique solution.*

Proof. According to the Lax-Milgram Lemma, it is sufficient to prove the boundedness and coercivity of $\alpha_N(\cdot, \cdot)$. For all $u, v \in \overline{V}^N$, we have

$$|\alpha_N(u, v)| \leq \gamma_1 (\nabla u, \nabla v)_N = \gamma_1 (\nabla u, \nabla v) \leq \gamma_1 \|u\|_1 \|v\|_1,$$

which implies $\alpha_N(\cdot, \cdot)$ is bounded.

The coercivity of $\alpha_N(\cdot, \cdot)$ follows from

$$|\alpha_N(u, u)| \geq \gamma_0 (\nabla u, \nabla u)_N = \gamma_0 (\nabla u, \nabla u) \geq \gamma_0 \|u\|_1^2.$$

\square

Appendix D. A concrete example of two-level block circulant matrix. We present a concrete example of an n -level block circulant matrix for the case of $d = 1$ and $n = 2$. First, consider the structures of vectors \mathbf{U} and \mathbf{F} . Note that

$$\mathbf{U} = (\mathbf{u}_0^T \ \mathbf{u}_1^T \ \cdots \ \mathbf{u}_{\frac{N}{2}-1}^T \ \mathbf{u}_{-\frac{N}{2}}^T \ \cdots \ \mathbf{u}_{-1}^T)^T,$$

where

$$\mathbf{u}_m = (\tilde{u}_{m,0}, \tilde{u}_{m,1}, \cdots, \tilde{u}_{m,\frac{N}{2}-1}, \tilde{u}_{m,-\frac{N}{2}}, \cdots, \tilde{u}_{m,-1})^T,$$

and

$$\mathbf{F} = (\tilde{\mathcal{F}}_0^T \ \tilde{\mathcal{F}}_1^T \ \cdots \ \tilde{\mathcal{F}}_{\frac{N}{2}-1}^T \ \tilde{\mathcal{F}}_{-\frac{N}{2}}^T \ \cdots \ \tilde{\mathcal{F}}_{-1}^T)^T,$$

where

$$\mathcal{F}_m = (\tilde{\mathcal{F}}_{m,0}, \tilde{\mathcal{F}}_{m,1}, \cdots, \tilde{\mathcal{F}}_{m,\frac{N}{2}-1}, \tilde{\mathcal{F}}_{m,-\frac{N}{2}}, \cdots, \tilde{\mathcal{F}}_{m,-1})^T.$$

From the discrete scheme (3.3), we have

$$\sum_{k_{\mathcal{U}} \in K_N^1} \tilde{\mathcal{A}}_{m,k_{\mathcal{A}}}(\mathbf{P}k_{\mathcal{V}})^T (\mathbf{P}k_{\mathcal{U}}) \tilde{\mathcal{U}}_{m,k_{\mathcal{U}}} = \tilde{\mathcal{F}}_{m,k_{\mathcal{V}}}, \quad k_{\mathcal{A}} = k_{\mathcal{V}} - k_{\mathcal{U}}, \quad k_{\mathcal{V}} = (m, k_{\mathcal{V}})^T, \quad k_{\mathcal{U}} = (m, k_{\mathcal{U}})^T.$$

Using the tensor-vector-index conversion, we obtain the first level circulant matrix \mathcal{A}_m defined by

$$\mathcal{A}_m = \begin{pmatrix} \tilde{\mathcal{A}}_{m,0} & \tilde{\mathcal{A}}_{m,-1} & \cdots & \tilde{\mathcal{A}}_{m,-\frac{N}{2}} & \tilde{\mathcal{A}}_{m,\frac{N}{2}-1} & \cdots & \tilde{\mathcal{A}}_{m,1} \\ \tilde{\mathcal{A}}_{m,1} & \tilde{\mathcal{A}}_{m,0} & \cdots & \tilde{\mathcal{A}}_{m,-\frac{N}{2}+1} & \tilde{\mathcal{A}}_{m,-\frac{N}{2}} & \cdots & \tilde{\mathcal{A}}_{m,2} \\ \vdots & \vdots & & \vdots & \vdots & \vdots & \vdots \\ \tilde{\mathcal{A}}_{m,\frac{N}{2}-1} & \tilde{\mathcal{A}}_{m,\frac{N}{2}-2} & \cdots & \tilde{\mathcal{A}}_{m,0} & \tilde{\mathcal{A}}_{m,-1} & \cdots & \tilde{\mathcal{A}}_{m,-\frac{N}{2}} \\ \tilde{\mathcal{A}}_{m,-\frac{N}{2}} & \tilde{\mathcal{A}}_{m,\frac{N}{2}-1} & \cdots & \tilde{\mathcal{A}}_{m,1} & \tilde{\mathcal{A}}_{m,0} & \cdots & \tilde{\mathcal{A}}_{m,-\frac{N}{2}+1} \\ \vdots & \vdots & & \vdots & \vdots & \vdots & \vdots \\ \tilde{\mathcal{A}}_{m,-1} & \tilde{\mathcal{A}}_{m,-2} & \cdots & \tilde{\mathcal{A}}_{m,\frac{N}{2}-1} & \tilde{\mathcal{A}}_{m,\frac{N}{2}-2} & \cdots & \tilde{\mathcal{A}}_{m,0} \end{pmatrix}.$$

Furthermore, by traversing m over the set K_N^1 , we obtain the second level block circulant matrix,

$$A = \begin{pmatrix} \mathcal{A}_0 & \mathcal{A}_{-1} & \cdots & \mathcal{A}_{-\frac{N}{2}} & \mathcal{A}_{\frac{N}{2}-1} & \cdots & \mathcal{A}_1 \\ \mathcal{A}_1 & \mathcal{A}_0 & \cdots & \mathcal{A}_{-\frac{N}{2}+1} & \mathcal{A}_{-\frac{N}{2}} & \cdots & \mathcal{A}_2 \\ \vdots & \vdots & & \vdots & \vdots & \vdots & \vdots \\ \mathcal{A}_{\frac{N}{2}-1} & \mathcal{A}_{\frac{N}{2}-2} & \cdots & \mathcal{A}_0 & \mathcal{A}_{-1} & \cdots & \mathcal{A}_{-\frac{N}{2}} \\ \mathcal{A}_{-\frac{N}{2}} & \mathcal{A}_{\frac{N}{2}-1} & \cdots & \mathcal{A}_1 & \mathcal{A}_0 & \cdots & \mathcal{A}_{-\frac{N}{2}+1} \\ \vdots & \vdots & & \vdots & \vdots & \vdots & \vdots \\ \mathcal{A}_{-1} & \mathcal{A}_{-2} & \cdots & \mathcal{A}_{\frac{N}{2}-1} & \mathcal{A}_{\frac{N}{2}-2} & \cdots & \mathcal{A}_0 \end{pmatrix}.$$

We observe that each matrix block \mathcal{A}_m is composed of the discrete Fourier coefficients of $\tilde{\mathcal{A}}_{(m,k_A)}$, exhibiting a circulant structure. By assembling these blocks, we construct the two-level block circulant matrix A .

Appendix E. PAM discretization.

Here, we utilize the PAM to discretize (2.8). We select functions $\alpha_p(\mathbf{x})$ and $f_p(\mathbf{x})$ with a period of L to approximate $\alpha(\mathbf{x})$ and $f(\mathbf{x})$, respectively. Define the following sets

$$\Lambda_{p,\alpha} = \{\mathbf{h}_\alpha = [L\boldsymbol{\lambda}_\alpha], \quad \boldsymbol{\lambda}_\alpha \in \Lambda_\alpha\},$$

$$\Lambda_{p,f} = \{\mathbf{h}_f = [L\boldsymbol{\lambda}_f], \quad \boldsymbol{\lambda}_f \in \Lambda_f\},$$

where $[\mathbf{x}] = ([x_1], \dots, [x_d])$. Then, we can express the Fourier series of $\alpha_p(\mathbf{x})$ and $f_p(\mathbf{x})$ as follows

$$\alpha_p(\mathbf{x}) = \sum_{\mathbf{h}_\alpha \in \Lambda_{p,\alpha}} \hat{\alpha}_p(\mathbf{h}_\alpha) e^{i(\mathbf{h}_\alpha^T \mathbf{x})/L}, \quad \hat{\alpha}_p(\mathbf{h}_\alpha) = \frac{1}{|\mathbb{T}^d|} \int_{\mathbb{T}^d} \alpha_p(\mathbf{x}) e^{-i(\mathbf{h}_\alpha^T \mathbf{x})/L},$$

$$f_p(\mathbf{x}) = \sum_{\mathbf{h}_f \in \Lambda_{p,f}} \hat{f}_p(\mathbf{h}_f) e^{i(\mathbf{h}_f^T \mathbf{x})/L}, \quad \hat{f}_p(\mathbf{h}_f) = \frac{1}{|\mathbb{T}^d|} \int_{\mathbb{T}^d} f_p(\mathbf{x}) e^{-i(\mathbf{h}_f^T \mathbf{x})/L},$$

where $\mathbb{T}^d = [0, 2\pi L)^d$. Similar to the quasiperiodic case, $\Lambda_{p,u} \subseteq \text{span}_{\mathbb{Z}} \{\Lambda_{p,\alpha}, \Lambda_{p,f}\}$, we then have

$$u_p(\mathbf{x}) = \sum_{\mathbf{h}_u \in \Lambda_{p,u}} \hat{u}_p(\mathbf{h}_u) e^{i(\mathbf{h}_u^T \mathbf{x})/L}, \quad \hat{u}_p(\mathbf{h}_u) = \frac{1}{|\mathbb{T}^d|} \int_{\mathbb{T}^d} u(\mathbf{x}) e^{-i(\mathbf{h}_u^T \mathbf{x})/L}.$$

Next, we discretize \mathbb{T}^d as

$$\mathbb{T}_N^d = \{\mathbf{x}_j = 2\pi(Lj_1/N, \dots, Lj_d/N) \in \mathbb{T}^d : 0 \leq j_1, \dots, j_d \leq N-1, \mathbf{j} = (j_1, \dots, j_d)\}.$$

This indicates that we distribute N points uniformly in each spatial direction of \mathbb{T}^d . As a result, there are a total of $E = N^d$ discrete points.

Similar to the definitions of the grid function space S_N and the inner product $(\cdot, \cdot)_N$ mentioned in Section 3, we can obtain the discrete Fourier coefficients of a periodic function $F(\mathbf{x})$ as follows

$$\tilde{F}(\mathbf{h}_F) = (F(\mathbf{x}_j), e^{i(\mathbf{h}_F^T \mathbf{x}_j)/L})_N = \frac{1}{E} \sum_{\mathbf{h}_F \in \Lambda_{p,F,N}} F(\mathbf{x}_j) e^{-i(\mathbf{h}_F^T \mathbf{x}_j)/L}, \quad \mathbf{x}_j \in \mathbb{T}_N^d,$$

where $\Lambda_{p,F,N} = \{\mathbf{h}_F : \mathbf{h}_F = [L\boldsymbol{\lambda}_F], \boldsymbol{\lambda}_F \in K_N^d\}$. Then we can apply PAM to discretize α_p, u_p, f_p , respectively,

$$\begin{aligned} \alpha_p(\mathbf{x}_j) &= \sum_{\mathbf{h}_\alpha \in \Lambda_{p,\alpha,N}} \tilde{\alpha}_p(\mathbf{h}_\alpha) e^{i(\mathbf{h}_\alpha^T \mathbf{x}_j)/L}, \quad \tilde{\alpha}_p(\mathbf{h}_\alpha) = \frac{1}{E} \sum_{\mathbf{h}_\alpha \in \Lambda_{p,\alpha,N}} \alpha_p(\mathbf{x}_j) e^{-i(\mathbf{h}_\alpha^T \mathbf{x}_j)/L}, \quad \mathbf{x}_j \in \mathbb{T}_N^d, \\ u_p(\mathbf{x}_j) &= \sum_{\mathbf{h}_u \in \Lambda_{p,u,N}} \tilde{u}_p(\mathbf{h}_u) e^{i(\mathbf{h}_u^T \mathbf{x}_j)/L}, \quad \tilde{u}_p(\mathbf{h}_u) = \frac{1}{E} \sum_{\mathbf{h}_u \in \Lambda_{p,u,N}} u_p(\mathbf{x}_j) e^{-i(\mathbf{h}_u^T \mathbf{x}_j)/L}, \quad \mathbf{x}_j \in \mathbb{T}_N^d, \\ f_p(\mathbf{x}_j) &= \sum_{\mathbf{h}_f \in \Lambda_{p,f,N}} \tilde{f}_p(\mathbf{h}_f) e^{i(\mathbf{h}_f^T \mathbf{x}_j)/L}, \quad \tilde{f}_p(\mathbf{h}_f) = \frac{1}{E} \sum_{\mathbf{h}_f \in \Lambda_{p,f,N}} f_p(\mathbf{x}_j) e^{-i(\mathbf{h}_f^T \mathbf{x}_j)/L}, \quad \mathbf{x}_j \in \mathbb{T}_N^d. \end{aligned}$$

To simplify the derivation, we introduce the notation $\tilde{\mathbf{h}}_\alpha = \mathbf{h}_\alpha/L \in \tilde{\Lambda}_{p,\alpha,N}$. Similarly, $\tilde{\mathbf{h}}_u$ and $\tilde{\mathbf{h}}_f$ are defined in the same manner.

Given a test function $v_p \in V^N := \text{span}\{e^{i\tilde{\mathbf{h}}_v^T \mathbf{x}} : \tilde{\mathbf{h}}_v \in \tilde{\Lambda}_{p,u,N}, \mathbf{x} \in \mathbb{T}^d\}$, the discrete variational formulation is to seek $u_p \in V^N$, such that the following holds

$$(\alpha_p \nabla u_p, \nabla v_p)_N = (f_p, v_p)_N \quad \forall v_p \in V^N.$$

From the orthogonality of base functions, we have

$$\begin{aligned} (\alpha_p \nabla u_p, \nabla v_p)_N &= \left(\sum_{\tilde{\mathbf{h}}_\alpha \in \tilde{\Lambda}_{p,\alpha,N}} \tilde{\alpha}_p(\tilde{\mathbf{h}}_\alpha) e^{i\tilde{\mathbf{h}}_\alpha^T \mathbf{x}_j} \sum_{\tilde{\mathbf{h}}_u \in \tilde{\Lambda}_{p,u,N}} (i\tilde{\mathbf{h}}_u^T) \tilde{u}_p(\tilde{\mathbf{h}}_u) e^{i\tilde{\mathbf{h}}_u^T \mathbf{x}_j}, (i\tilde{\mathbf{h}}_v^T) e^{i\tilde{\mathbf{h}}_v^T \mathbf{x}_j} \right)_N \\ &= \left(\sum_{\tilde{\mathbf{h}} = \tilde{\mathbf{h}}_\alpha + \tilde{\mathbf{h}}_u} \sum_{\tilde{\mathbf{h}}_u \in \tilde{\Lambda}_{p,u,N}} \tilde{\alpha}_p(\tilde{\mathbf{h}}_v - \tilde{\mathbf{h}}_u) \tilde{u}_p(\tilde{\mathbf{h}}_u) (i\tilde{\mathbf{h}}_u^T) e^{i\tilde{\mathbf{h}}_u^T \mathbf{x}_j}, (i\tilde{\mathbf{h}}_v^T) e^{i\tilde{\mathbf{h}}_v^T \mathbf{x}_j} \right)_N \\ &= \sum_{\tilde{\mathbf{h}}_u \in \tilde{\Lambda}_{p,u,N}} \tilde{\alpha}_p(\tilde{\mathbf{h}}_v - \tilde{\mathbf{h}}_u) \tilde{u}_p(\tilde{\mathbf{h}}_u) (\tilde{\mathbf{h}}_v^T \tilde{\mathbf{h}}_u), \\ (f_p, v_p)_N &= \left(\sum_{\tilde{\mathbf{h}}_f \in \tilde{\Lambda}_{p,f,N}} \tilde{f}_p(\tilde{\mathbf{h}}_f) e^{i\tilde{\mathbf{h}}_f^T \mathbf{x}_j}, e^{i\tilde{\mathbf{h}}_v^T \mathbf{x}_j} \right)_N = \tilde{f}_p(\tilde{\mathbf{h}}_v), \end{aligned}$$

that is

$$\sum_{\tilde{\mathbf{h}}_u \in \tilde{\Lambda}_{p,u,N}} \tilde{\alpha}_p(\tilde{\mathbf{h}}_v - \tilde{\mathbf{h}}_u) \tilde{u}_p(\tilde{\mathbf{h}}_u) (\tilde{\mathbf{h}}_v^T \tilde{\mathbf{h}}_u) = \tilde{f}_p(\tilde{\mathbf{h}}_v).$$

Similar to the quasiperiodic case, we can employ tensor-vector-index conversion to generate the linear system. Define

$$A = (A_{ij}) \in \mathbb{C}^{E \times E}, \quad A_{ij} = \tilde{\alpha}_p(\tilde{\mathbf{h}}_v - \tilde{\mathbf{h}}_u)^N,$$

$$W = (W_{ij}) \in \mathbb{C}^{E \times E}, \quad W_{ij} = \tilde{\mathbf{h}}_v^T \tilde{\mathbf{h}}_u,$$

where indices i, j are determined by

$$(E.1) \quad \mathbf{h}_v \xrightarrow{\mathcal{C}} i, \quad \mathbf{h}_u \xrightarrow{\mathcal{C}} j,$$

respectively. The column vectors \mathbf{U} and \mathbf{F} are defined by

$$\mathbf{U} = (U_j) \in \mathbb{C}^E, \quad U_j = \tilde{u}_p(\tilde{\mathbf{h}}_u),$$

$$\mathbf{F} = (F_i) \in \mathbb{C}^E, \quad F_i = \tilde{f}_p(\tilde{\mathbf{h}}_v).$$

Finally, we obtain the following linear system for PAM

$$Q\mathbf{U} = \mathbf{F}, \quad Q = A \circ W \in \mathbb{C}^{E \times E}.$$

Appendix F. Solving corrector equation by the PM. In this section, we are concerned about the two-dimensional quasiperiodic corrector equation

$$(F.1) \quad -\operatorname{div}(A_{\text{q-per}}(\mathbf{x})(\mathbf{p} + \nabla u_{\mathbf{p}}(\mathbf{x}))) = 0,$$

where $\mathbf{p} = \mathbf{e}_i, i = 1, 2$. We apply PM to obtain $u_{\mathbf{e}_i}$ and calculate the homogenized coefficient A^* using the formula

$$(F.2) \quad A_{ij}^* = \mathcal{M} \{ \mathbf{e}_i^T A_{\text{q-per}}(\mathbf{x})(\mathbf{e}_j + \nabla u_{\mathbf{e}_j}(\mathbf{x})) \}.$$

We assume that

$$A_{\text{q-per}}(\mathbf{x}) = \begin{pmatrix} \alpha(\mathbf{x}) & 0 \\ 0 & \beta(\mathbf{x}) \end{pmatrix},$$

where $\alpha(\mathbf{x}), \beta(\mathbf{x})$ have the same projection matrix $\mathbf{P} = (\mathbf{P}_1, \mathbf{P}_2)^T \in \mathbb{P}^{2 \times n}$. (F.1) can be split into two separate equations

$$(F.3) \quad -\operatorname{div}(A_{\text{q-per}}(\mathbf{x})\nabla u_{\mathbf{e}_1}(\mathbf{x})) = f_1(\mathbf{x}),$$

$$(F.4) \quad -\operatorname{div}(A_{\text{q-per}}(\mathbf{x})\nabla u_{\mathbf{e}_2}(\mathbf{x})) = f_2(\mathbf{x}),$$

where

$$f_1(\mathbf{x}) = \partial_{x_1} \alpha(\mathbf{x}), \quad f_2(\mathbf{x}) = \partial_{x_2} \beta(\mathbf{x}).$$

We only derive the discrete scheme for (F.3), while the scheme for (F.4) follows a similar approach.

Applying PM to discretize (F.3), we have

$$\alpha(\mathbf{x}_j) = \sum_{\mathbf{k}_\alpha \in K_N^n} \tilde{\alpha}(\mathbf{k}_\alpha) e^{i(\mathbf{P}\mathbf{k}_\alpha)^T \mathbf{x}_j} \quad \mathbf{x}_j \in X_{\mathbf{P}},$$

$$\begin{aligned}
\beta(\mathbf{x}_j) &= \sum_{\mathbf{k}_\beta \in K_N^n} \tilde{\alpha}(\mathbf{k}_\beta) e^{i(\mathbf{P}\mathbf{k}_\beta)^T \mathbf{x}_j}, \quad \mathbf{x}_j \in X_P, \\
u_{e_1}(\mathbf{x}_j) &= \sum_{\mathbf{k}_{u_{e_1}} \in K_N^n} \tilde{u}_{e_1}(\mathbf{k}_{u_{e_1}}) e^{i(\mathbf{P}\mathbf{k}_{u_{e_1}})^T \mathbf{x}_j}, \quad \mathbf{x}_j \in X_P, \\
f_1(\mathbf{x}_j) &= \sum_{\mathbf{k}_{f_1} \in K_N^n} \tilde{f}_1(\mathbf{k}_{f_1}) e^{i(\mathbf{P}\mathbf{k}_{f_1})^T \mathbf{x}_j}, \quad \mathbf{x}_j \in X_P.
\end{aligned}$$

Given any test function $v \in V^N := \text{span} \left\{ e^{i(\mathbf{P}\mathbf{k}_v)^T \mathbf{x}}, \mathbf{x} \in \mathbb{R}^2, \mathbf{k}_v \in K_N^n \right\}$, the discrete variational formulation is to seek $u_{e_1} \in V^N$ with $\tilde{u}_{e_1}(\mathbf{0})$, such that

$$(A_{\text{q-per}} \nabla u_{e_1}, \nabla v)_N = (f_1, v)_N.$$

In consideration of the orthogonality of basis functions, we have

$$\begin{aligned}
& (A_{\text{q-per}} \nabla u_{e_1}, \nabla v)_N \\
&= \left(\begin{pmatrix} \sum_{\mathbf{k}_\alpha \in K_N^n} \tilde{\alpha}(\mathbf{k}_\alpha) e^{i(\mathbf{P}\mathbf{k}_\alpha)^T \mathbf{x}_j} & 0 \\ 0 & \sum_{\mathbf{k}_\beta \in K_N^n} \tilde{\beta}(\mathbf{k}_\beta) e^{i(\mathbf{P}\mathbf{k}_\beta)^T \mathbf{x}_j} \end{pmatrix} \begin{pmatrix} \sum_{\mathbf{k}_{u_{e_1}} \in K_N^n} \tilde{u}_{e_1}(\mathbf{k}_{u_{e_1}}) (\imath \mathbf{P}_1 \mathbf{k}_{u_{e_1}}) e^{i(\mathbf{P}\mathbf{k}_{u_{e_1}})^T \mathbf{x}_j} \\ \sum_{\mathbf{k}_{u_{e_1}} \in K_N^n} \tilde{u}_{e_1}(\mathbf{k}_{u_{e_1}}) (\imath \mathbf{P}_2 \mathbf{k}_{u_{e_1}}) e^{i(\mathbf{P}\mathbf{k}_{u_{e_1}})^T \mathbf{x}_j} \end{pmatrix} \right. \\
&\quad \left. \begin{pmatrix} (\imath \mathbf{P}_1 \mathbf{v}) e^{i(\mathbf{P}\mathbf{k}_v)^T \mathbf{x}_j} \\ (\imath \mathbf{P}_2 \mathbf{v}) e^{i(\mathbf{P}\mathbf{k}_v)^T \mathbf{x}_j} \end{pmatrix} \right)_N \\
&= \left(\begin{pmatrix} \sum_{\mathbf{k}_\alpha \in K_N^n} \tilde{\alpha}(\mathbf{k}_\alpha) e^{i(\mathbf{P}\mathbf{k}_\alpha)^T \mathbf{x}_j} & \sum_{\mathbf{k}_{u_{e_1}} \in K_N^n} \tilde{u}_{e_1}(\mathbf{k}_{u_{e_1}}) (\imath \mathbf{P}_1 \mathbf{k}_{u_{e_1}}) e^{i(\mathbf{P}\mathbf{k}_{u_{e_1}})^T \mathbf{x}_j} \\ \sum_{\mathbf{k}_\beta \in K_N^n} \tilde{\beta}(\mathbf{k}_\beta) e^{i(\mathbf{P}\mathbf{k}_\beta)^T \mathbf{x}_j} & \sum_{\mathbf{k}_{u_{e_1}} \in K_N^n} \tilde{u}_{e_1}(\mathbf{k}_{u_{e_1}}) (\imath \mathbf{P}_2 \mathbf{k}_{u_{e_1}}) e^{i(\mathbf{P}\mathbf{k}_{u_{e_1}})^T \mathbf{x}_j} \end{pmatrix}, \begin{pmatrix} (\imath \mathbf{P}_1 \mathbf{k}_v) e^{i(\mathbf{P}\mathbf{k}_v)^T \mathbf{x}_j} \\ (\imath \mathbf{P}_2 \mathbf{k}_v) e^{i(\mathbf{P}\mathbf{k}_v)^T \mathbf{x}_j} \end{pmatrix} \right)_N \\
&= \sum_{\mathbf{k}_{u_{e_1}} \in K_N^n} \tilde{\alpha}(\mathbf{k}_v - \mathbf{k}_{u_{e_1}})^N \tilde{u}_{e_1}(\mathbf{k}_{u_{e_1}}) (\mathbf{P}_1 \mathbf{k}_v)^T (\mathbf{P}_1 \mathbf{k}_{u_{e_1}}) + \sum_{\mathbf{k}_{u_{e_1}} \in K_N^n} \tilde{\beta}(\mathbf{k}_v - \mathbf{k}_{u_{e_1}})^N \tilde{u}_{e_1}(\mathbf{k}_{u_{e_1}}) (\mathbf{P}_2 \mathbf{k}_v)^T (\mathbf{P}_2 \mathbf{k}_{u_{e_1}}),
\end{aligned}$$

$$(f_1, v)_N = \left(\sum_{\mathbf{k}_{f_1} \in K_N^n} \tilde{f}_1(\mathbf{k}_{f_1}) e^{i(\mathbf{P}\mathbf{k}_{f_1})^T \mathbf{x}_j}, e^{i(\mathbf{P}\mathbf{k}_v)^T \mathbf{x}_j} \right)_N = \tilde{f}_1(\mathbf{k}_v),$$

that is

$$\begin{aligned}
& \sum_{\mathbf{k}_{u_{e_1}} \in K_N^n} \tilde{\alpha}(\mathbf{k}_v - \mathbf{k}_{u_{e_1}})^N \tilde{u}_{e_1}(\mathbf{k}_{u_{e_1}}) (\mathbf{P}_1 \mathbf{k}_v)^T (\mathbf{P}_1 \mathbf{k}_{u_{e_1}}) + \\
& \sum_{\mathbf{k}_{u_{e_1}} \in K_N^n} \tilde{\beta}(\mathbf{k}_v - \mathbf{k}_{u_{e_1}})^N \tilde{u}_{e_1}(\mathbf{k}_{u_{e_1}}) (\mathbf{P}_2 \mathbf{k}_v)^T (\mathbf{P}_2 \mathbf{k}_{u_{e_1}}) = \tilde{f}_1(\mathbf{k}_v).
\end{aligned}$$

Define

$$A^1 = (A_{ij}^1) \in \mathbb{C}^{D \times D}, \quad A_{ij}^1 = \tilde{\alpha}(\mathbf{k}_v - \mathbf{k}_{u_{e_1}})^N,$$

$$\begin{aligned}
A^2 &= (A_{ij}^2) \in \mathbb{C}^{D \times D}, \quad A_{ij}^2 = \tilde{\beta}(\mathbf{k}_v - \mathbf{k}_{u_{e_1}})^N, \\
W^1 &= (W_{ij}^1) \in \mathbb{C}^{D \times D}, \quad W_{ij}^1 = (\mathbf{P}_1 \mathbf{k}_v)^T (\mathbf{P}_1 \mathbf{k}_{u_{e_1}}), \\
W^2 &= (W_{ij}^2) \in \mathbb{C}^{D \times D}, \quad W_{ij}^2 = (\mathbf{P}_2 \mathbf{k}_v)^T (\mathbf{P}_2 \mathbf{k}_{u_{e_1}}),
\end{aligned}$$

where indices i, j are determined by

$$(F.5) \quad \mathbf{k}_v \xrightarrow{C} i, \quad \mathbf{k}_{u_{e_1}} \xrightarrow{C} j,$$

respectively. The column vectors \mathbf{U} and \mathbf{F} are defined, respectively, by

$$\mathbf{U} = (U_j) \in \mathbb{C}^D, \quad U_j = \tilde{u}_{e_1}(\mathbf{k}_{u_{e_1}}),$$

$$\mathbf{F} = (F_i) \in \mathbb{C}^D, \quad F_i = \tilde{f}_1(\mathbf{k}_v).$$

Consequently, we obtain the following linear system

$$Q\mathbf{U} = \mathbf{F}, \quad Q = A^1 \circ W^1 + A^2 \circ W^2 \in \mathbb{C}^{D \times D}.$$

To derive the discrete scheme of (F.4), we replace f_1 to f_2 and obtain the linear system in the same way. The homogenized coefficients are then obtained by clarifying the formula (5.2)

$$(F.6) \quad A_{11}^* = \mathcal{M} \{ \alpha(\mathbf{x}) \nabla_{x_1} u_{e_1}(\mathbf{x}) + \alpha(\mathbf{x}) \},$$

$$(F.7) \quad A_{12}^* = \mathcal{M} \{ \alpha(\mathbf{x}) \nabla_{x_1} u_{e_2}(\mathbf{x}) \},$$

$$(F.8) \quad A_{21}^* = \mathcal{M} \{ \beta(\mathbf{x}) \nabla_{x_2} u_{e_1}(\mathbf{x}) \},$$

$$(F.9) \quad A_{22}^* = \mathcal{M} \{ \beta(\mathbf{x}) \nabla_{x_2} u_{e_2}(\mathbf{x}) + \beta(\mathbf{x}) \}.$$

Appendix G. More numerical experiments.

G.1. Three incommensurate frequencies. Consider the quasiperiodic elliptic equation with

$$\alpha_2(x) = \cos(2\pi x) + \cos(2\pi\sqrt{2}x) + \cos(2\pi\sqrt{3}x) + 6$$

and

$$u_3(x) = \sin(2\pi x) + \sin(2\pi\sqrt{2}x) + \sin(2\pi\sqrt{3}x).$$

The numerical solutions are denoted as u_N , where N represents the number of discrete points in each dimension. We utilize the \mathcal{L}^2 -norm to quantify the numerical error $e_N = \|u_N - u\|_{\mathcal{L}^2}$, where $u = u_3$ is the exact solution of (2.8).

C-PCG vs. PCG in PM scheme. We apply the PM with the C-PCG method to solve the quasiperiodic elliptic equation (2.8) and compare its efficiency with that of the PCG method. Table 10 compares the efficiency of PCG with C-PCG. It is evident that C-PCG can significantly reduce CPU time compared to PCG. At the same time, C-PCG achieves substantial memory savings, as illustrated in Table 11. Visually, as shown in Figure 7, the ratio $r = M_{\text{PCG}}/M_{\text{C-PCG}}$ is approximately $\mathcal{O}(D)$. For comparison, when $N = 32$, C-PCG requires only 1.25e-01 Gb of memory,

N	4	8	16	32	64
CPU time(PCG)	4.31e-02	2.76	-	-	-
CPU time(C-PCG)	4.10e-03	3.12e-02	2.51e-01	2.05	15.87
Iteration(PCG)	20	24	-	-	-
Iteration(C-PCG)	20	24	24	23	23
e_N (PCG)	7.79e-02	6.16e-16	-	-	-
e_N (C-PCG)	7.79e-02	6.16e-16	8.10e-16	1.88e-15	1.86e-15

Table 10: Efficiency comparison of PCG and C-PCG when solving (2.8) with $(\alpha_2(x), u_3(x))$ in PM (Data for $N \geq 16$ with PCG is not available due to insufficient memory).

N	4	8	16	32	64
M_{PCG}	1.60e-02	1.00e+00	6.40e+01	4.10e+03	2.62e+05
$M_{\text{C-PCG}}$	2.44e-04	2.00e-03	1.56e-02	1.25e-01	1.00e+00

Table 11: Comparison between M_{PCG} and $M_{\text{C-PCG}}$.

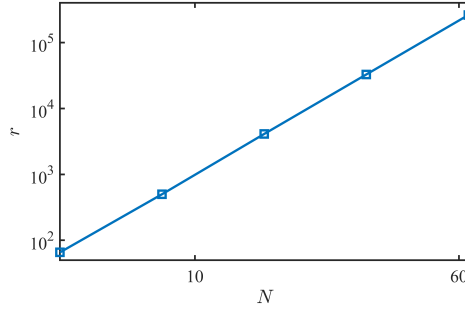


Fig. 7: The ratio $r = M_{\text{PCG}}/M_{\text{C-PCG}}$ vs. N in log-log scale.

N	4	8	16	32	64
Q	3.88e+01	1.56e+02	6.25e+02	2.50e+03	5.61e+04
QM	3.27	3.27	3.13	3.07	3.09

Table 12: Condition number of Q and preconditioned system QM .

whereas PCG requires 4.10e+03 Gb. This results in the memory consumed by the two reaching $32800 \approx 32^3$. Moreover, Table 12 presents the performance of preconditioner M . The condition number of Q undergoes a substantial reduction and stabilizes in the range of 3 to 3.5 as N grows after applying M .

PM vs. PAM. We also present the numerical results of PAM. We select periodic functions $\alpha_{2p}(x) = \cos(2\pi x) + \cos(2\pi([\sqrt{2}L]/L)x) + \cos(2\pi([\sqrt{3}L]/L)x) + 6$ to approximate $\alpha_2(x)$. The corresponding Diophantine approximation error e_d is given by

$$e_d = \max \left\{ \sqrt{2}L - [\sqrt{2}L], \sqrt{3}L - [\sqrt{3}L] \right\}.$$

We take $E = 16L$ in the PAM to ensure enough numerical accuracy of discretizing (2.8). Table 13 records the numerical error e_N of PAM and corresponding Diophantine approximation error e_d . The data shows that e_N of PAM is mainly controlled by e_d . Moreover, once L is fixed, the discrete points achieve a critical value, the numerical error e_N of PAM cannot decrease, as illustrated in Table 14. For example, when we set $L = 34$, despite the increase in k , the numerical error of PAM remains at 1.17e-01.

N	3×16	7×16	22×16	34×16	41×16
$\lfloor \sqrt{2}L \rfloor / L$	4/3	10/7	31/22	48/34	58/41
$\lfloor \sqrt{3}L \rfloor / L$	5/3	12/7	38/22	59/34	71/41
e_d	2.43e-01	1.24e-01	1.13e-01	1.10e-01	1.72e-02
e_N	2.63e-01	1.75e-01	1.96e-01	1.175e-01	2.87e-02

Table 13: Numerical error of PAM in solving (2.8) with $\alpha_{2p}(x)$ and corresponding Diophantine approximation error against L .

e_N	$k = 3$	$k = 4$	$k = 5$	$k = 6$
$L = 3$	2.62e-01	2.62e-01	2.63e-01	2.63e-01
$L = 7$	1.75e-01	1.75e-01	1.75e-01	1.75e-01
$L = 22$	1.96e-01	1.96e-01	1.96e-01	1.96e-01
$L = 34$	1.17e-01	1.17e-01	1.17e-01	1.17e-01
$L = 41$	2.87e-02	2.87e-02	2.87e-02	2.87e-02

Table 14: Numerical error with variable $E = L \times 2^k$ for different L in PAM.

Finally, we compare the efficiency of PM and PAM. Table 15 presents the accuracy achieved by PM and PAM, along with their required CPU time. Moreover, Figure 8 provides a visual representation of the trade-off between cost and accuracy. It showcases that PM achieves machine precision in a short amount of time, while PAM only achieves relatively low accuracy dependent on the Diophantine approximation error, even with much larger CPU time.

	N	4	8	16
e_N	PM	7.79e-02	6.16e-16	8.10e-16
	PAM($L = 1183$)	2.56e-01	2.79e-03	2.79e-03
	PAM($L = 1463$)	2.55e-01	2.25e-03	2.25e-03
CPU time	PM	3.99e-02	2.59e-02	2.51e-01
	PAM($L = 1183$)	4.56	17.26	70.23
	PAM($L = 1463$)	5.43	21.34	81.63

Table 15: Performance comparison between PM and PAM in solving (2.8) with $\alpha_2(x)$.

Different frequencies in coefficient and exact solution. We now consider the case where the spectral points of coefficients and solutions are distinct. We discretize (2.8) using the PM with $\alpha_1(x) = \cos(2\pi x) + \cos(2\pi\sqrt{2}x) + 6$ and the exact solution $u_4(x) = \sin(2\pi x) + \sin(2\pi\sqrt{3}x)$, and solve the resulting linear system using the C-PCG method. This quasiperiodic system can thus be embedded into a three-dimensional parent system. The numerical results demonstrate that the numerical error e_N of the PM can quickly reach machine precision, as shown in Table 16.

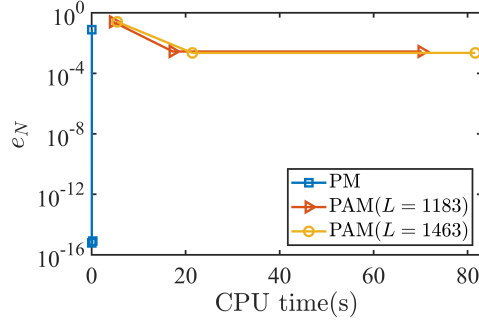


Fig. 8: Cost-Accuracy trade-off of PM and PAM ($L = 1183, 1463$) in solving (2.8) with $\alpha_2(x)$, respectively.

N	4	8	16	32	64
CPU time	3.70e-03	2.51e-02	2.47e-01	1.10	8.69
Iteration	20	24	24	23	23
e_N	7.10e-02	6.26e-16	7.95e-16	1.79e-15	1.74e-15

Table 16: Numerical solution of (2.8) with $(\alpha_1(x), u_4(x))$ using C-PCG method in PM.

G.2. Four incommensurate frequencies. In this subsection, we further demonstrate that the PM is a high-precision and efficient algorithm to solve (2.8) through the two-dimensional example. Consider the case where $\alpha_3(x, y) = \cos(2\pi x) + \cos(2\pi\sqrt{2}y) + \cos(2\pi\sqrt{3}x) + \sin(2\pi\sqrt{5}y) + 12$ and $u_5(x, y) = \sin(2\pi x) + \cos(2\pi\sqrt{2}y) + \sin(2\pi\sqrt{3}x) + \cos(2\pi\sqrt{5}y)$ in (2.8). Table 17 shows that e_N can achieve machine precision within a short time.

N	4	6	8
e_N	4.25e-02	2.41e-16	5.39e-16
CPU time	0.31	1.57	4.97

Table 17: Numerical solution with $(\alpha_3(x, y), u_5(x, y))$ using PM with C-PCG method.